Master thesis of University of Ulsan

The effect of knee varus deformity on cartilage and meniscus loading and screw fixation stability after high tibia osteotomy investigation using finite element analysis

The graduate school of University of Ulsan

Department of Mechanical Engineering

Huan Liu

The effect of knee varus deformity on cartilage and meniscus loading and screw fixation stability after high tibia osteotomy investigation using finite element analysis

Supervisor: Professor Young-Jin Yum

A Dissertation

Submitted to

the Graduate School of University of Ulsan

In partial Fulfillment of the Requirements

for the Degree of

Master of Engineering

by

Huan Liu

Department of Mechanical Engineering

University of Ulsan, Ulsan, Korea

Jun 2020

LIU HUAN의 공학석사학위 논문을 인준함

심사위원장 주석재 

심사위원 천두만 

심사위원 염영진 

울산대학교 대학원

2020 년 6 월

The effect of knee varus deformity on cartilage and meniscus loading and screw fixation stability after high tibia osteotomy investigation using finite element analysis

This certifies that the dissertation of
Liu Huan is approved by

Committee Chairman Prof. Seok-Jae Chu Seokjae Chu

Committee Member Prof. Doo-Man Chun

Committee Member Prof. Young-Jin Yum Young J. Yum

Department of Mechanical Engineering
University of Ulsan, Ulsan, South Korea
Jun 2020

ACKNOWLEDGMENTS

First and foremost, I want to express my heartfelt gratitude to my advisor professor Young-Jin Yum, whose patient guidance, valuable suggestions, and constant encouragement in academic studies. Without his invaluable help and generous encouragement, the present thesis would not have been accomplished.

Besides, I would like to thank all the professors in the school of mechanical engineering at Ulsan University, thanks to their great knowledge that I have learned. I would also express my gratitude to the committee members: Prof. Seok-Jae Chu and Prof. Doo-Man Chun for evaluating my research work.

Last but not least, I would like to express my special thanks to my parents who have always been helping me out of difficulties and supporting without a word of complaint.

Ulsan , Repulic of Korea

Jun 2020

Huan Liu

ABSTRACT

Osteoarthritis (OA) is a common disease among older people, affecting about 237 million people, almost 3.3% of the world's population. High tibia open-wedge osteotomy (HTO) is a popular surgery method to treat medial compartment osteoarthritis of the knee with varus deformity. Tomo-fix system composed of titanium plate and titanium screw always be used to fix the open-wedge. One intact normal knee model was developed to be used to investigate the biomechanical environment change of the knee with a varus angle. Another after-HTO tibia model fix with the TomoFix plate was developed to be used to investigate the fixation stability when missing one locking screw located at the upper portion of the open-wedge. The results of this study indicated that the varus deformity strongly influences the stress and contact pressure distribution on knee medial and lateral compartment, it could be the risk factor of OA. TomoFix plate fixation stability and biomechanical environment are all slightly influenced by the absence of screw A, B, or C, However, missing locking screw D will be the risk factor of hinge breakage

CONTENTS

ACKNOWLEDGMENTS.....v

ABSTRACT vi

LIST OF FIGURES ix

CHAPTER 1: Introduction.....1

1.1 Normal knee joint anatomy structure and biomechanics 3

1.1.1 normal knee joint anatomy structure 3

1.12 The normal knee biomechanics 5

1.2 OA knee and biomechanics 6

1.2.1 OA knee anatomy structure 6

1.2.2 OA knee biomechanics.....7

1.3 Research background 7

1.3.1 Application of finite element analysis in orthopedic biomechanical simulation 7

1.3.2 knee joint biomechanics FEM studies and clinical studies 8

1.4 The main content, innovation, and significance of this study 10

1.4.1 The main content of this study.....10

1.4.2 Significances of this study 11

1.4.3 Innovation points of this study 11

Chapter 2 High Tibial Osteotomy(HTO).....12

2.1 Introduction.....13

2.2 Varus and valgus malalignment of lower limb 14

2.3 Medial open wedge high tibial osteotomy procedure 16

2.4 The TomoFix fixation system.....19

Chapter 3 Model and methods 21

3.1 CT and MRI scan.....22

3.2 knee joint modeling.....22

3.3 FE model 30
3.3.1 Material properties 30
3.3.2 Loading and boundary conditions 32
Chapter 4 Results and discussion **35**
4.1 Model validation 36
4.2 Results and discussion 38
4.2.1 Topic I 38
4.2.2 Topic II 57
Chapter 5 Conclusions and future work **62**
5.1 Conclusion 63
5.2 Future work 64
Reference **65**

LIST OF FIGURES

Fig. 1-1 The knee joint anatomical structure 3
Fig. 1-2 The soft tissue structure of the knee 4
Fig. 1-3 OA knee anatomy structure 6
Fig. 2-1 HTO x-ray image 14
Fig. 2-2 The mechanical axis of lower limb 15
Fig. 2-3 Varus and valgus deformity 15
Fig. 2-4 Correction angle determination 16
Fig. 2-5 Hing point and Safety zone 17
Fig. 2-6 Correction angle and joint line check with X-ray 18
Fig. 2-7 TomoFix plate 18
Fig. 2-8 Trigonometric chart 19
Fig. 3-1 CT and MR image 23
Fig. 3-2 Bone and soft tissues segmentation 24
Fig. 3-3 Reconstructed bone and soft tissue models 25
Fig. 3-4 Model registration 26
Fig. 3-5 Netural alimental model 27
Fig. 3-6 KJLO angle 28
Fig. 3-7 Intact netural alignmental knee joint model 29
Fig. 3-8 HTO model 29
Fig. 3-9 Reference point 30
Fig. 3-10 Mesh model used in this study 31
Fig. 3-11 Rotation center for femur 31
Fig. 3-12 Load and boundary condition 34
Fig. 4-1 Comparison of interfragmentary movement 37
Fig. 4-2 Meniscus indexes comparison between normal and varus knee 39
Fig. 4-3 Von Mises stress distribution on meniscus 41
Fig. 4-4 Contact pressure distribution on meniscus 42

Fig. 4-5 Pressive stress distribution on meniscus 43
Fig. 4-6 Shear stress distribution on meniscus..... 44
Fig. 4-7 Femur cartilage indexes comparison 46
Fig. 4-8 Von Mises stress distribution on femur cartilage 47
Fig. 4-9 Contact pressure distribution on femur cartilage 48
Fig. 4-10 Compressive stress distribution on femur cartilage 49
Fig. 4-11 Shear stress distribution on femur cartilage 50
Fig. 4-12 Tibia cartilage indexes comparison..... 52
Fig. 4-13 Von Mises stress distribution on tibia cartilage..... 53
Fig. 4-14 Contact pressure distribution on tibia cartilage..... 54
Fig. 4-15 Compressive stress distribution on tibia cartilage..... 55
Fig. 4-16 Shear stress distribution on tibia cartilage..... 56
Fig. 4-17 Maximum von Mises stress..... 57
Fig. 4-18 Micromotion of the opening wedge 58
Fig. 4-19 Von Mises stress distribution on TomoFix plate and bone..... 59
Reference 65

CHAPTER 1: Introduction

Osteoarthritis (OA) is a common disease among older people, affecting about 237 million people, almost 3.3% of the world's population [1]. The most common symptoms are joint pain, stiffness, joint swelling, and decreased range of motion [2]. It is recognized that the etiology of OA is multifactorial and complicated, such as age, obesity, joint soft tissue injury, arthrosis congenital abnormality, and malformation, etc [3]. The OA patients are unable to move freely and can not work properly due to the symptoms of OA, besides, the cost of treatment imposes a considerable economic burden on families and the social system.

For early OA, Symptoms can be effectively relieved by medication, but, joint soft tissue damage regularly occurred for intermediate and advanced OA. Thus, knee arthroplasty always is considered as the ultimate treatment plan to relieve the patient's pain, however, the surgical injury to the knee is irreversible. The artificial joint service life, surgery cost are also can be considerable factors.

High tibia open-wedge osteotomy (HTO) as a new knee preservation therapy was been first introduced by Jackson and Waugh in 1961. HTO is a realignment surgy that designed to reduce the load on the medial compartment through changing the weight from the medial side to the lateral side. Nowadays, HTO becomes popular to treat medial compartment osteoarthritis of the knee with varus deformity.

Tomo-fix system is composed of titanium plate and titanium screw that intended for osteotomies, treatment of bone and joint deformities, fixation of fractures, and malalignment caused by injury or disease, thus, Tomo-fix system always been used in HTO surgery procedure.

1.1 Normal knee joint anatomy structure and biomechanics

1.1.1 normal knee joint anatomy structure

The knee is the largest joint and one of the most important joints in the human body. It plays an essential role in movement related to carrying the body weight in horizontal and vertical directions. The knee joint consists of bony structures such as the tibia, femur, fibula, patella, etc and non-bone structures such as the meniscus, articular cartilage, ligament, muscle, joint capsule, and synovial membrane.

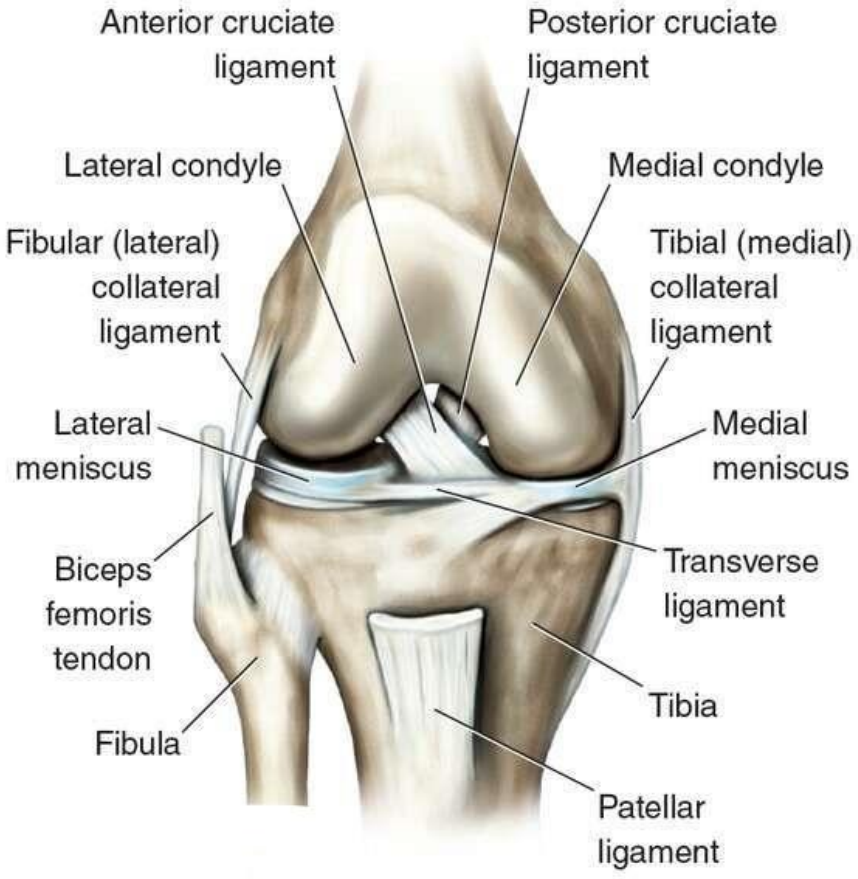

Fig. 1-1 The knee joint anatomical structure

The bone structure of the knee includes tibia, femur, patella, and fibula. The femoral condyle and tibial plateau formed the tibiofemoral joint, patella and femoral trochlear formed the patellofemoral joint. The distal femur and distal tibia are covered

by femoral cartilage and tibial cartilage respectively, the thickness of the normal articular cartilage is approximately 2-5mm. Articular cartilage contributes to enlarge the knee load-bearing surface and distributes force uniformly when the knee is under loading. It also has a good lubricating effect that contributes to reduce joint wear and increase joint flexibility, besides, articular cartilage has a good absorption effect that is conducive to buffer stress effect, thus protect the knee joint from injury during strenuous exercise.

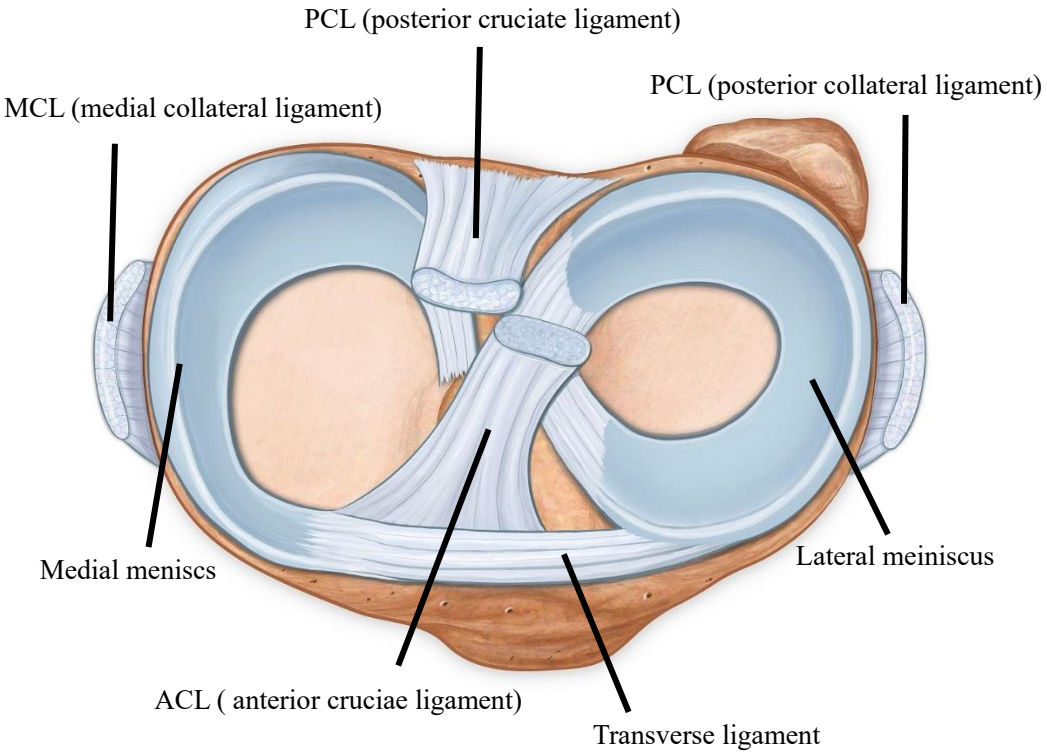

Fig. 1-2 the soft tissue structure of the knee

The meniscus is located between the femoral condyle and tibial plateau, the cross-section is triangular and the outside is thicker than inside. It is concave on the top and flat on the bottom, the shape is anastomosis with femoral condyle and tibial plateau respectively, it increased the kinetic stability of femoral and tibial plateau anterior horn and posterior horn of meniscus are articulating with the tibial plateau, lateral meniscus presents an o-shape, the middle portion is slightly wider than anterior and posterior portion, medial meniscus presents a c-shape, the posterior portion is wider

than anterior portion, as shown in Fig 1-2. The meniscus is an elastic tissue that contributes to buffering gravity and protects the joint surface from impact.

Knee joint ligament includes ACL, PCl, MCL, and LCL. ACL and PCL are located in the articular cavity, articulating with the lateral, medial femoral condyle and tibial intercondylar eminence. LCL located at the posterior-lateral side of the knee joint originates from the lateral femoral epicondyle, attaching to the head of the fibula. MCL located at the posterior-medial side of the knee joint, originates from the medial femoral epicondyle, attaching to the medial tibial condyle, as shown in Fig 1-1. The ligament is capable of preventing femur, tibia dislocation and remaining stability of the knee in motion.

1.12 The normal knee biomechanics

As introduced in 1.1.1, the knee anatomy structure determines its biomechanics complexity when the knee under loading. The load on the knee joint varies with motion and gait pattern. There is no bending moment and muscle strength, the static force is 0.43 times the body weight when the knee is in standing posture, however, the force could be 2-3 times the body weight when walking, besides, it could be bigger when walking fast or go upstairs and downstairs. The meniscus transfer almost 100% of the knee joint load when knee joint under a small load, however, it transfer 70% of the knee joint load when knee joint under a big load.

The femur generated an adductive motion when the knee in gait, under loading, thus, the medial compartment bears 50% more load than the lateral compartment, but the contact surface is bigger than the lateral compartment, thus, the contact pressure may be same with lateral side. Meniscus contributes to transfer joint force, increasing joint contact area when the knee is under big loading, meanwhile, the meniscus deformation improved the compliance of the joint surface, avoids stress concentration when knee joint bearing big stress.

1.2 OA knee and biomechanics

1.2.1 OA knee anatomy structure

OA (osteoarthritis) is a common chronic disease, knee joint structure is extremely complicated, it is easy to be injured during strenuous motion, thus, the knee joint is one of the high incidences of OA. Epidemiological studies indicated that almost 6% of the people suffer OA after 30 years old and it increased to 13% after 60% years old [4,5]. The incidence rate of knee OA will increase with the aging rate increases. OA has become a considerable issue in our social system.

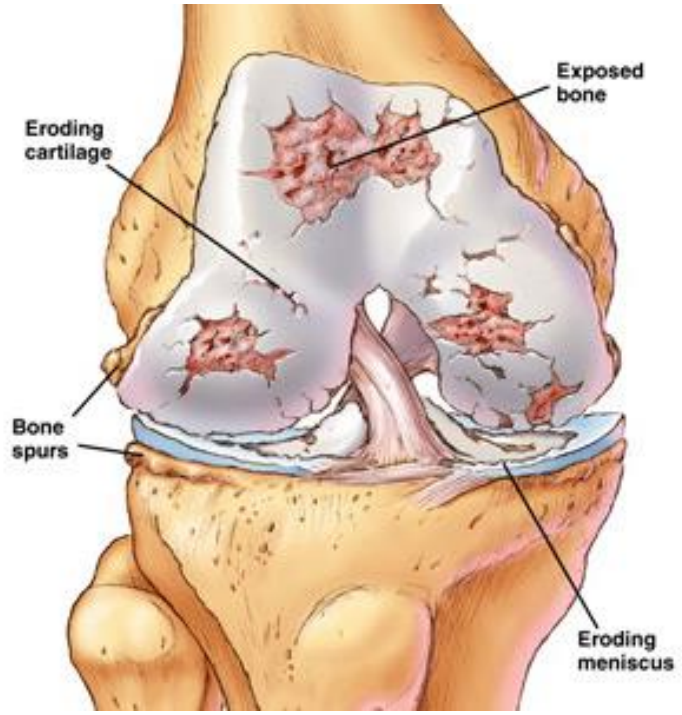

Fig. 1-3 OA knee anatomy structure

Bone spurs, cartilage eroding, bone exposing, meniscus eroding, joint space reducing, etc, are the main pathological manifestations of OA knee, as shown in Fig. 1-3. There are 5 levels of knee OA according to radiological diagnostic criteria [6]: level 0: the normal knee; level I: the joint space slightly reduced, may have bone spurs; level II: have bone spurs, joint space reduced; level III: have moderate bone spurs, joint space significantly reduced, cartilage slightly subchondral sclerosis; level IV:

have massive bone spurs, joint space significantly reduced, cartilage severe subchondral sclerosis, knee joint deformity, and swelling.

1.2.2 OA knee biomechanics

Some biomechanical factors, such as lower limb force line change, overloading, overuse, and malalignment, etc, are considered the main factors which caused OA [7]. The joint space angle increased, medial compartment joint space is smaller than the lateral compartment, the mechanical axis moved to the medial side, thus, stress concentration occurred in the medial compartment joint surface, this stress damages the medial side cartilage that is responding to the phenomenon which the medial compartment OA patient is more than lateral compartment OA, besides, meniscus and cartilage degeneration contributes to decreasing the tibiofemoral joint contact area, increase the fraction force and accelerate the joint surface wear.

1.3 Research background

1.3.1 Application of finite element analysis in orthopedic biomechanical simulation

Biomechanics is by using mechanical principles and methods to investigate the mechanical problems of an organism, also used for clinical diagnosis and treatment.

Courant pioneered FEM(finite element method) in 1943, the finite element method was used for aircraft structure analysis by Tumor in 1956 [8], whereafter, FEM is widely used in aerospace, transportation, and chemistry, etc. FEM was firstly used in orthopedic biomechanics by Brekelmans in 1972 [9], since then, the research field which used FEM is expanding, such as, bone stress analysis, fracture fixation, optimization of artificial joint structure, etc. At that time, most of the studies just build a simple 2D FE model to do stress analysis due to the limitation of computer and software technology [10,11]. After decades of development of computer and software technology, it is possible to process large volume data, in recent years, many

researchers built the 3D geometric model and mesh model that consider the main anatomical structures, meanwhile, FEM theory and software are also improving, it is easier to build a complicated FE model and get the FE solution.

Nowadays, the application of FEM in orthopedic biomechanics no longer limited to do stress analysis, also used in the time-dependent biomechanical characterization, prosthesis design, implant optimization, mechanical wear of the prosthesis, biological processes and pathological changes, finite element analysis is well applied.

1.3.2 knee joint biomechanics FEM studies and clinical studies

Until now, a lot of research results have been achieved about knee biomechanics behavior using FEM. Bendjaballah el al [12] reconstructed a tibiofemoral joint which includes four major ligaments to study the contact stress of varus/valgus knee. Donahue et al [13] built a 3D knee joint model to investigate the influence of femur rotation and flexion on tibiofemoral joint contact behavior. Dong et al [14] reconstructed bony and non-bony structure by using CT (computer tomography) and MRI (magnetic resonance imaging) respectively, building a 3D FE model which was used to study the stress variation on articular cartilage surface when cartilage defect is enlarged, the simulation results were used to guide the operative treatment of OA patients. Nattapon et al [15] built 3 normal knee and 3 OA knee FE models, obtained the stress distribution on articular cartilage, analysis the biomechanics difference between the normal knee and OA knee. Ji et al [16] built a 3D knee joint FE model, mimic the clinical partial/total meniscectomy, obtained the stress and contact area of articular cartilage, study the influence of different operation plans on knee degeneration. Homyk et al [17] by using FEM, built 3D FE models to ligamentous injury of varus/valgus deformity, they indicated that the stress on ACL of varus knee is 83% higher than the valgus knee. E. pena et al [18] reconstructed a full knee joint model include the main bony structure, joint cartilages, and ligaments, applied 1150 N compressive load and 134 anterior-posterior loads to the tibia to validate the 3D FE model.

And in the meanwhile, lots of researchers by using FEM to investigated the biomechanics of prosthesis and HTO fixation system. Applied the research results to the design and structure optimization of the prosthesis, guiding the clinical HTO operation. Yong-gon Koh et al [19] built an intact 3D knee joint model and mimic clinical HTO procedure to investigate the effect of the Tomo-fix plate composed of different materials. Yen-Nien Chen et al [20] built an HTO knee joint 3D FE model fixed with Tomo-fix system to study the mechanical stability of HTO with locking plate and various length, type of titanium fix screws. Yang et al [21] designed a new type of spherical prosthesis and established FE model, applied a 2800 N compressive load to investigated the stress on polyethylene liner when the prosthesis rotation angle is 0°,4°, 8°, verified the new design is more reasonable than the traditional design. Tomaso et al [22] built a knee prosthesis FE model, studied the contact area and stress between the prosthesis under different load and flexion angles, besides, compared with the results obtained by Fuji film. Bischoff et al [23] built knee prosthesis FE model investigated the stress, contact pressure, contact area on knee prosthesis when ascending/descending stairs, and during normal walking. Marjan et al [24] investigated the stress distribution on femur after femoral cartilage replacement surgery which the NiTi alloy was used as the cartilage substitute material with the finite element method.

There are many previous clinical studies investigated the effect of knee joint line obliquity after HTO and knee arthroplasty through checking the lower lamb mechanical line with X-ray images or use experimental method [25-28]. But, there are few studies to evaluate the effect of knee joint line obliquity on knee joint soft tissues with FEM (finite element method). The clinical study takes several years to track the patients and can not evaluate the biomechanical change visually, however, FEM can resolve all the limitations of the clinical study. Besides, all the previous studies about screw fixation stability after HTO applied all locking screws[19, 20, 29] but in some special cases that tibial plateau fracture or proximal tibial fracture has happened years ago and then, not all the locking screws can be applied. This study aimed to evaluate the effect of knee joint line obliquity on the meniscus, articular

cartilage, and the fixation stability of TomoFix system when missing one locking screw.

1.4 The main content, innovation, and significance of this study

1.4.1 The main content of this study

There are two topics in this study, the topic I is about the joint line obliquity, and topic II is about screw fixation stability under different fix conditions.

Topic I

1. Scan the left leg of one male young volunteer (age: 29 years old, height: 175cm, weight: 70Kg, has no history of knee injury) to get the computerized tomography (CT) images and magnetic resonance images. Reconstructing the bony structure and soft tissues based on the image data, and then build seven intact knee solid models that three models with a varus angle, three models with joint line reverse obliquity angle, and one model is in the natural alignment condition.

2. Build the FE model base on the reconstructed solid models. Define the materials and boundary conditions of each FE model and then do simulation. Obtain the Von Mises stress and shear stress on soft tissues of each model.

3. Compare the simulation result of each model, evaluate the influence of the varus deformity

Topic II

1. Reconstructing the tibia and fibula bone base on the CT image data. Create an opening wedge on the medial side of the tibia to mimic the HTO procedure and then fix it with the TomoFix plate under different fix conditions.

2. Build the FE model base on the solid model. Define the materials and boundary conditions of each FE model and then do simulation. Obtain the Von mises stress on bone and TomoFix plate of each model.

3. Compare the simulation result of each model to evaluate the influence of when missing one locking screw.

1.4.2 Significances of this study

The knee joint is one of the important joints of the human body and it also is the joint peculiarly prone to disease. Numerous researchers study the knee joint due to the significance and application values in prosthesis design and clinical diagnosis and treatment. Significance of this study are the following:

1. Developing the method of 3D reconstruction base on image data which contributes to observing the pathological tissue visually for an orthopedist and better communication with patients. 3D reconstruction method also conduces to OA clinical diagnosis and making a treatment plan.

2. Investigating the biomechanical environment change of knee use FE analysis. Illuminating the evolvement mechanism between biomechanical change and joint deformity. It can be the theoretical basis of redistributing the stress load on the knee joint, slowing the progression of OA through various interventions in early OA.

3. Studying the biomechanical change of OA progression. Illuminating the biomechanical osteogenesis in OA progression contributes to guiding the orthodontic bracket design and knee osteotomy.

4. Evaluating the fixation stability of the TomoFix plate in special cases.

1.4.3 Innovation points of this study

1. Developed an intact normal knee joint 3D model based on CT&MR image data. Resolved the matching problem between bone and soft tissues.
The modeling method not only appropriate for the normal knee but also suitable for OA knee.

2. Build OA knee models by adding boundary conditions in Abaqus.

3. Established a complete evaluation system to analyze the biomechanical difference between the normal knee and OA knee.

4. It is the first time to evaluate the fixation stability of the TomoFix plate in special cases.

Chapter 2 High Tibial Osteotomy(HTO)

2.1 Introduction

High tibia osteotomy is an orthopedic surgery to treat unicompartmental osteoarthritis(OA) by shifting the weight-bearing line from the lesion side to the no-lesion side. In doing this, HTO can realign the lower limb mechanical axis and decreasing the stress on the lesion side thereby restoring the knee joint function [30].

HTO was first to be introduced by Jackson and Wangh [31] in 1961. They reported that ten patients underwent HTO and all patient's joint pain was relieved. High tibial osteotomy to correct the OA knee became popular after Coventry [32] reported favorable outcomes. Lateral close wedge and medial open wedge (Fig.2-1) are two representative osteotomies of HTO [33,34]. Nowadays HTO was widely used because of its advantages. One advantage of HTO is that it can preserve the knee anatomy. A successful osteotomy may delay the need for a joint replacement for several years. Another advantage is that there are no restrictions on physical activities after an osteotomy. The patient will be able to participate in favorite activities, even high-impact exercise.

As introduced in the previous section, HTO includes the media open wedge and the lateral close wedge osteotomy. For a medial compartment OA patient, choosing one suitable surgery procedure is a debated issue [35]. Comparing to lateral close wedge HTO, the media open wedge HTO became more popular and widely acceptable. There are several limitations of lateral close wedge HTO [36, 37]:

1. Fibular osteotomy or proximal tibiofibular joint disruption
2. Lateral muscle detachment
3. Personal nerve dissection
4. Bone stock loss
5. More demanding subsequent TKR(total knee replacement)

This study focus on medial open wedge HTO, thus all the model will be cut an open wedge in the medial tibia side follow the surgery procedure under the guidance of an orthopedist.

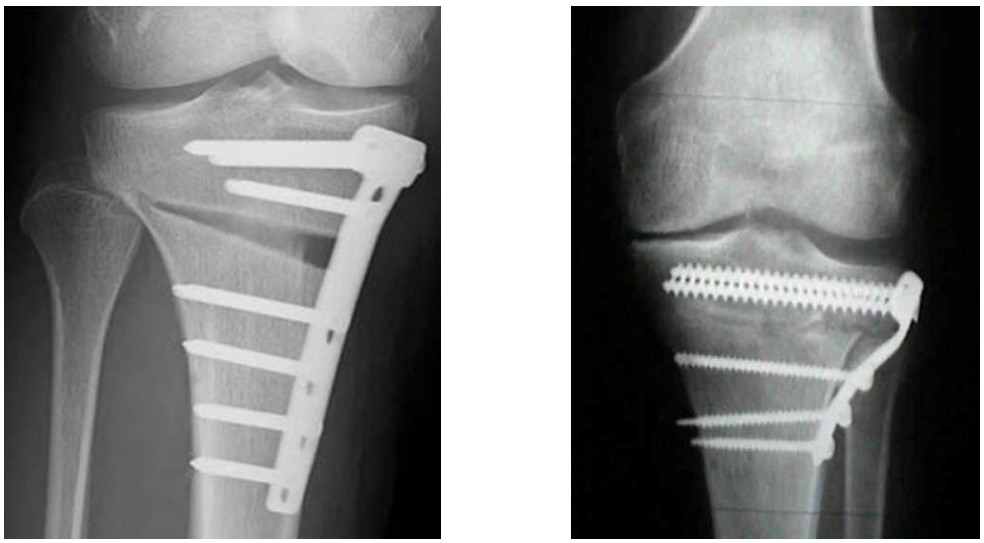

(a) (b)

Fig. 2-1 (a): medial open wedge HTO (b): lateral close wedge HTO

2.2 Varus and valgus malalignment of lower limb

The alignment of the lower limb is defined by the hip-knee-ankle (HKA) angle (Fig. 2-2), it influences the load distribution and the cross position of the weight-bearing line [38]. The HKA angle is the lateral angle formed by the mechanical axis of femur and tibia. The fumer mechanical axis id the line from the femur head center to the center of the knee joint and the tibia mechanical axis is the line from the knee center to the center of the ankle joint. The HKA angle is approximately 180 degrees when the knee is neutral aligned. The HKA angle of the valgus and varus knee is >180 degrees and < 180 degrees, respectively.

The varus and valgus knee also can be estimated by the cross position of the weight-bearing line (Fig. 2-3). When the lower limb is in standing position, the line from the femur head center to the center of the ankle joint is named weight-bearing line. For a neutrally aligned knee, the weight-bearing line almost coincides with the HKA line. The weight-bearing line of varus knee crosses the medial side of the tibial plateau while it crosses the lateral side of the tibial plateau for a valgus knee. The load distribution on the tibial plateau will be imbalance due to varus or valgus deformity.

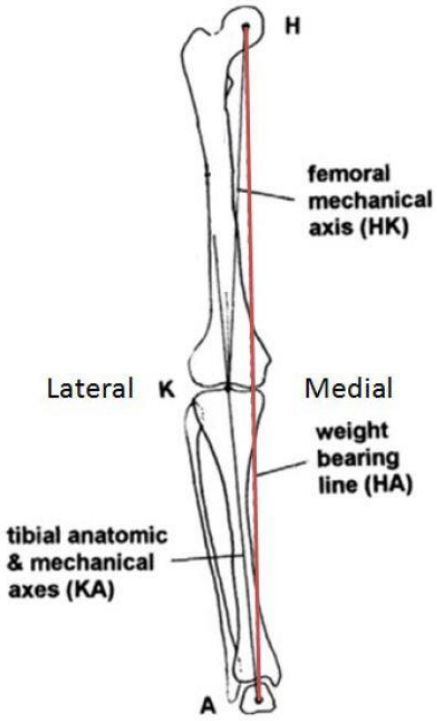

Fig. 2-2 The mechanical axis of lower limb

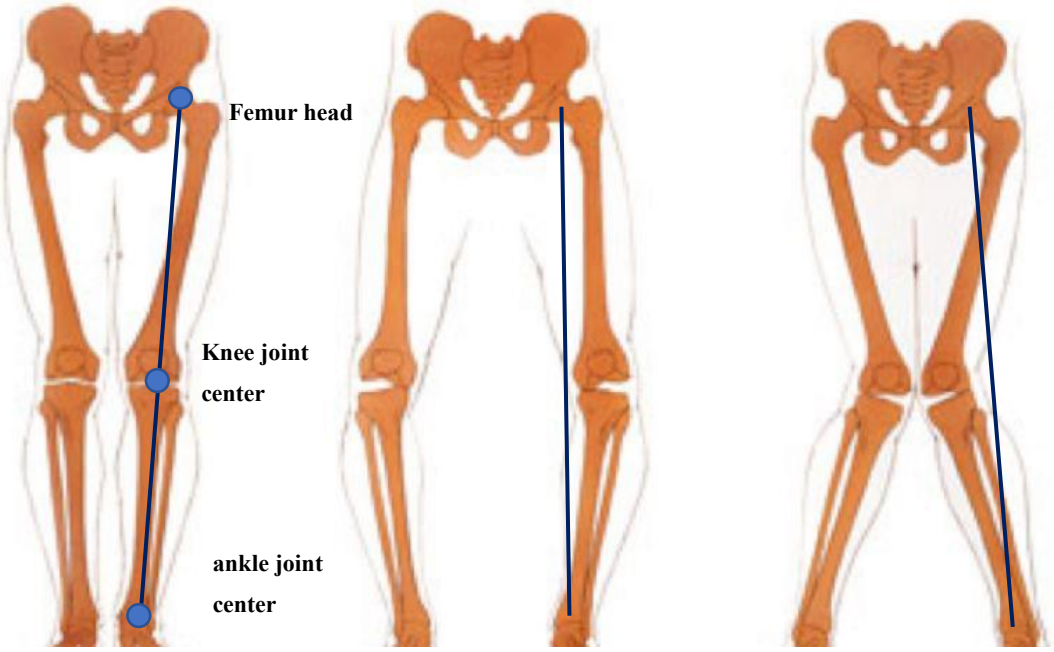

(a) (b) (c)

Fig. 2-3 (a): neutral alignment (b): varus deformity (c): valgus deformity

2.3 Medial open wedge high tibial osteotomy procedure

A precise preoperative plan is crucial to the success of this procedure. The recommended method for planning is that of Miniaci [39]. It must be done based on the weight-bearing x-ray of the full leg in the Anterior-Posterior view, either on paper or at a digital workstation. The medial open wedge osteotomy procedure [40] as follows:

1. Determine the mechanical axis of the leg: Draw a straight line from the center of the femoral head to the center of the ankle joint (Fig. 2-4).
2. Draw the new weight-bearing line from the center of the femoral head, passing the joint line through the desired position (Fig. 2-4).
3. Determine a hinge point (h). The optimal position of the hinge point may vary according to patient-specific anatomy. Rotate the leg 30° internally to identify the optimal hinge point. The lateral hinge point should be within the proximal 1/3 of the fibular head (safety zone)(Fig. 2-5) [41].
4. Connect the hinge point h (Fig. 2-5) with the center of the Ankle joint (a). Rotate the connecting line h-a like a circle until it crosses the new weight-bearing line. Connect the crossing point (b) with the hinge point h. The angle between the connecting line h-a and h-b is the angle of opening (a). Transfer the opening angle (a) to the level of the planned osteotomy. The height at the medial cortex (o) is the height of the opening.
5. Check the leg axis and joint line with a full leg X-ray after cutting an opening wedge (Fig. 2-5).
6. Fix with TomoFix plate (Fig. 2-6).

Determine the entry point of the transverse osteotomy. It lies just above the pes anserinus. Make sure there is still enough space for the proximal part of the TomoFix plate (holes A-D) so that the screw in hole D can be inserted without protruding into the opening gap. Depending on the determined opening angle and the length of the Osteotomy cut (mediolateral diameter of the osteotomy) the corresponding opening height can be derived from Hernigou's trigonometric chart (Fig. 2-7).

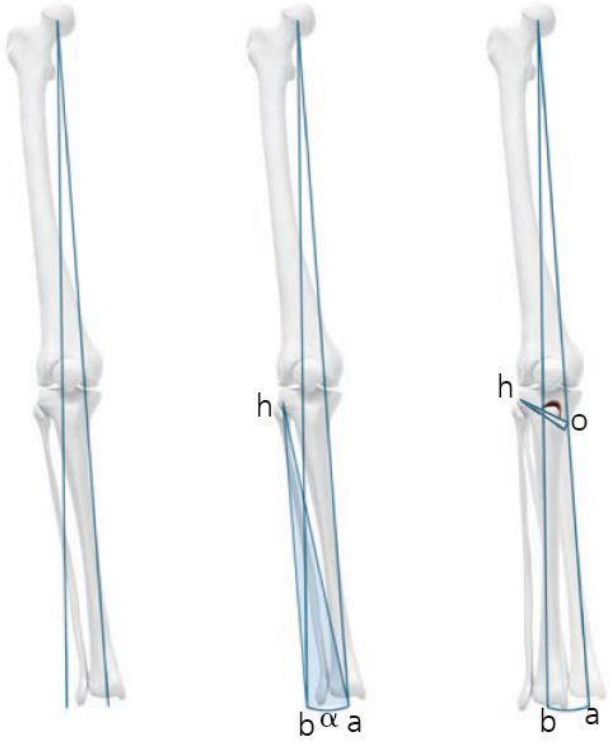

Fig. 2-4 Correction angle determination

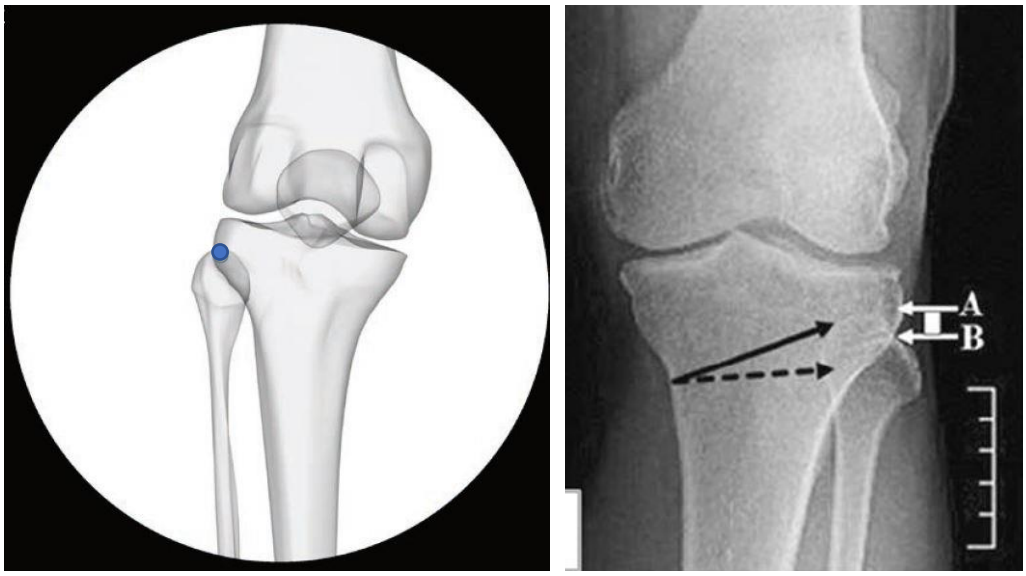

(a) (b)

Fig. 2-5 (a): Hing point (b): Safety zone

Fig. 2-5 Correction angle and joint line check with X-ray

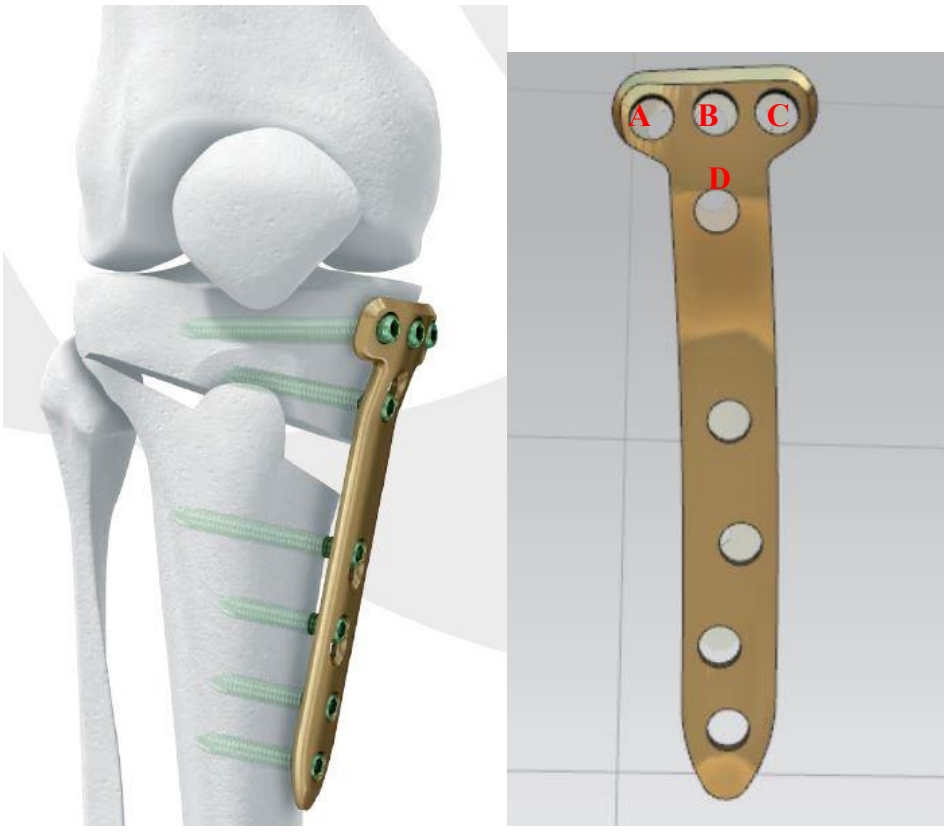

(a) (b)

Fig. 2-6 (a): After-HTO tibia fix with TomoFix plate (b): TomoFix plate

Trigonometric chart

Mediolateral diameter of the osteotomy (mm)	Correction Angle															
	4°	5°	6°	7°	8°	9°	10°	11°	12°	13°	14°	15°	16°	17°	18°	19°
50 mm	3	4	5	6	7	8	9	10	10	11	12	13	14	15	16	16
55 mm	4	5	6	7	8	9	10	10	11	12	13	14	15	16	17	18
60 mm	4	5	6	7	8	9	10	11	12	14	15	16	17	18	19	20
65 mm	5	6	7	8	9	10	11	12	14	15	16	17	18	19	20	21
70 mm	5	6	7	8	10	11	12	13	15	16	17	18	20	21	22	23
75 mm	5	6	8	9	10	12	13	14	16	17	18	20	21	22	24	25
80 mm	6	7	8	10	11	13	14	15	17	18	19	21	22	24	25	26

Fig. 2-7 Trigonometric chart

2.4 The TomoFix fixation system

There are several types of fixation systems that are used in medial opening wedge HTO. These system options include a combination of locked or unlocked, short or long, and the presence or absence of a metal block (tapered or rectangular) [42]. The TomoFix plate (TomoFix Osteotomy system; Depuy Synthes, West Chester, PA, USA) is widely used because of its good fixation stability and biomechanical properties [43]. A long and rigid T-shaped titanium plate with an internal locking fixation system is considered the gold standard [44].

Titanium alloy has good rigidity. Some studies have indicated that the stress on fixed screws and the TomoFix plate is much higher than that on the bone after HTO. In other words, the TomoFix fixation system may cause delayed bone union due to the stress shielding effect [45, 46]. Gotz Roderer et al. used a human cadaver knee joint specimen to compare the maximum interfragmentary movement and stress on screws and plates after the opening wedge was fixed with a dynamic locking screw versus a traditional locking screw. The group found that the dynamic locking screw can provide more micromotion, and create a better biomechanical environment for bone healing than can a traditional locking screw [47]. Pei-Wei Weng et al. created several FE tibia models with different correction angles that were fixed with the

TomoFix system and investigated the fixation stability under different load conditions [48].

The TomoFix fixation system consists of one T-shape plate and eight locking screws. Almost all of the specimens or FE models in the previous studies included all of the locking screws; however, in certain cases in which the tibial plateau fracture or proximal tibial fracture happened years prior, all of the locking screws cannot be applied to the upper portion of the opening wedge. Therefore, there is a need to evaluate the fixation stability and stress on the screws, plates and bones in such special cases due to the increased risk of complications, broken screws, and a long recovery period when a locking screw is missing.

However, it is difficult to explore the internal stress of screws, bones, plates and the interfragmentary micromotions of the opening wedge, because there is no sensor that is small enough to be inserted into the human body without disturbing the hardware. However, the finite element (FE) method and numerical simulation can avoid the limitations of prior studies [49-52]. This study also sought to evaluate the fixation stability and biomechanical environment when one screw is missing at the upper portion of the opening wedge. To do so, we used a validated after-HTO FE tibia model fixed with the TomoFix fixation system.

Chapter 3 Model and methods

3.1 CT and MRI scan

This study aims to build an intact knee model include all bony structure, main ligaments, menisci, and articular cartilages to quantify the stress on the knee joint soft tissues under different varus angle and joint line obliquity. We also use the model which remove all soft tissues and femur bone fix with TomoFix plate to investigate the stress distribution and fixation stability. Thus, an accurate model is extremely important. The cartilage and menisci of the patient who is undergoing unicompartmental OA are not intact and can not be distinguished easily in the MR (Magnetic Resonance) image due to massive joint effusion. Therefore, a volunteer without knee joint injury history was been selected for this study (Height: 175 cm; weight: 70 Kg).

Reconstructing an accurate anatomical model becomes possible using CT (Computer Tomography) or MR images with the development of high-resolution CT and MR imaging techniques. The contour of the interest region can be segmented manually or automatically based on the grey value. This grey value is associate with the bone mineral density in CT image, can be used to reconstruct the bony structure. MR uses the same principles with CT, however, MR provides better details in soft tissues. Thus, this study uses the CT and MR images of the same human to develop all the anatomical structures.

During the CT and MR scan, the left leg of the volunteer at full extension position. We scanned the full leg from ankle joint to femoral head, the slice thickness was set to 1mm, we got 1040 slices CT images (axial plane). Only the tibiofemoral joint is scanned during the MR scan due to the limitation of the MR machine's field of view. The slice thickness was set to 1 mm, a total of 440 slices MR images were generated (axial plane 170 slices, coronal plane 150 slices, sagittal plane 120 slices).

3.2 knee joint modeling

All of the CT images were imported into mimics software (version: 21.0, materialize NV, Leuven, Belgium). The contours of the bone were sketched in each

section by examining the relatively higher gray value compared to that of the other surrounding soft tissues and muscles. The bony contours were calculated to get the surface model after the smoothing mask. The small holes were filled in the mask manually. However, the bone model surface was not smooth enough. Therefore, one suitable smooth factor must be defined to smooth the surface. A lot of bony anatomical detail stands to be lost if the smooth factor is too big. In contrast, the bone model surfaces will still be rough if the smooth factor is too small. The tibia's cortical bone and cancellous bone were demarcated according to their gray value in the same way that was previously mentioned.

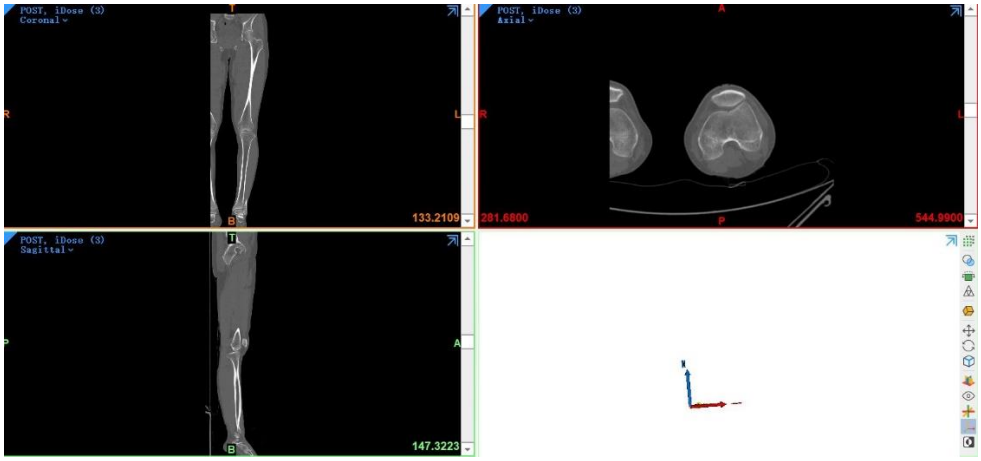

(a)

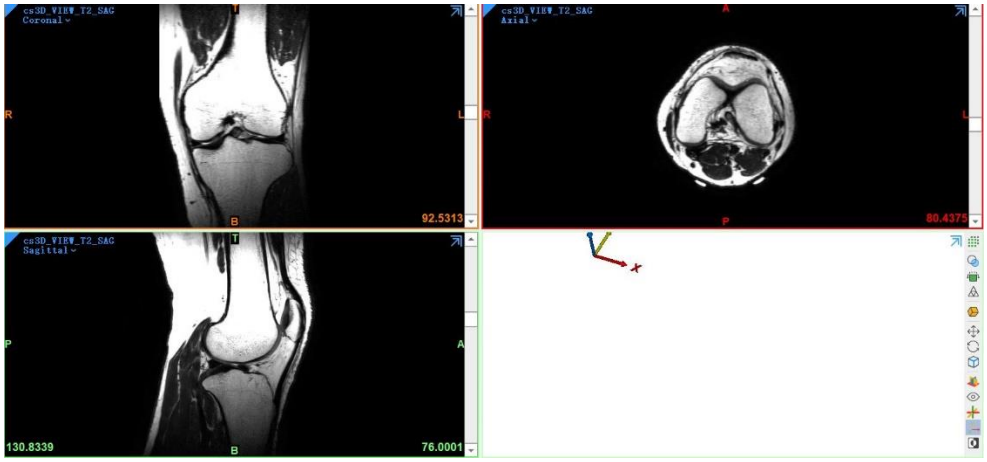

(b)

Fig.3-1 CT and MR image (a): CT images in Mimics software (b): MR images Mimics software

All the MR images were imported into Mimics software, segmented all the bony structure (tibia, femur, fibula, patella) and soft tissues (ACL: anterior cruciate ligament; PCL: posterior cruciate ligament; MCL: medial collateral ligament; LCL: lateral collateral ligament; femoral cartilage, medial tibial cartilage, lateral tibial cartilage, medial meniscus, lateral meniscus, tibial-fibula cartilage). All the models formed in Mimics based on the image data are shell models.

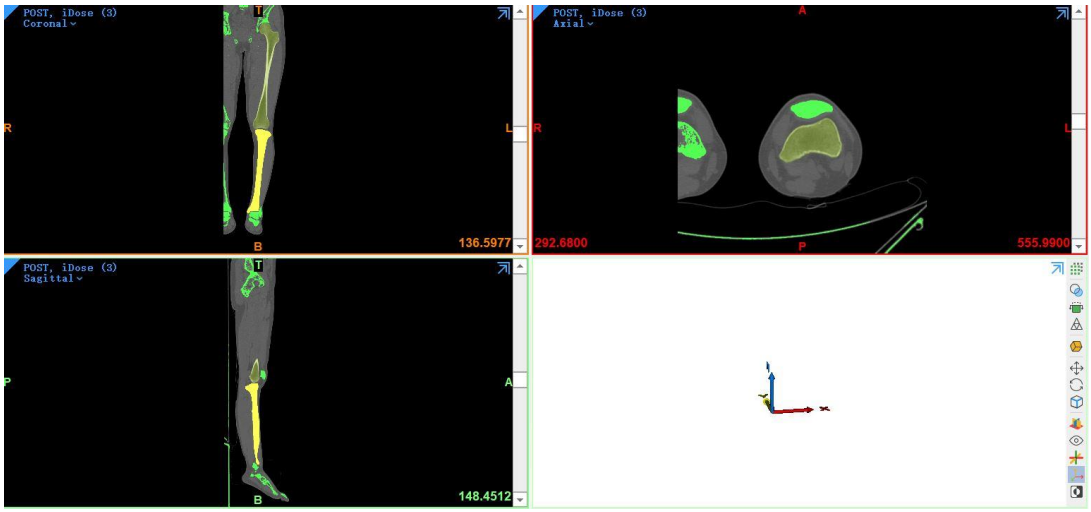

(a)

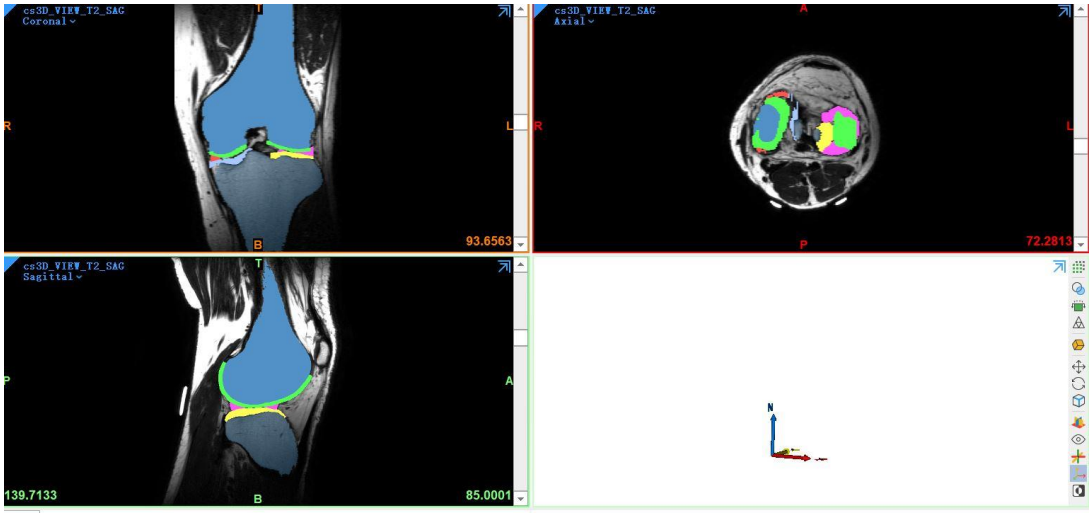

(b)

Fig. 3-2 Bone and soft tissues segmentation (a): Bone segmentation (b): Soft tissues segmentation

All the shell models that were formed in the Mimics were imported into 3-Matic software (version: 13.0, materialize NV, Leuven, Belgium). Using this software, we optimized the shell surface through fixing, reducing, and remesh function. The bone 3D geometrical structure was outputted in step format.

The point cloud data of the TomoFix fixation system (1 T-shape plate and 8 locking screws) were obtained using a 3D scanner machine. These data were imported into the Geomagic DesignX software (version: 2016, 3D systems Korea, Soul, Republic of Korea) to form solid models.

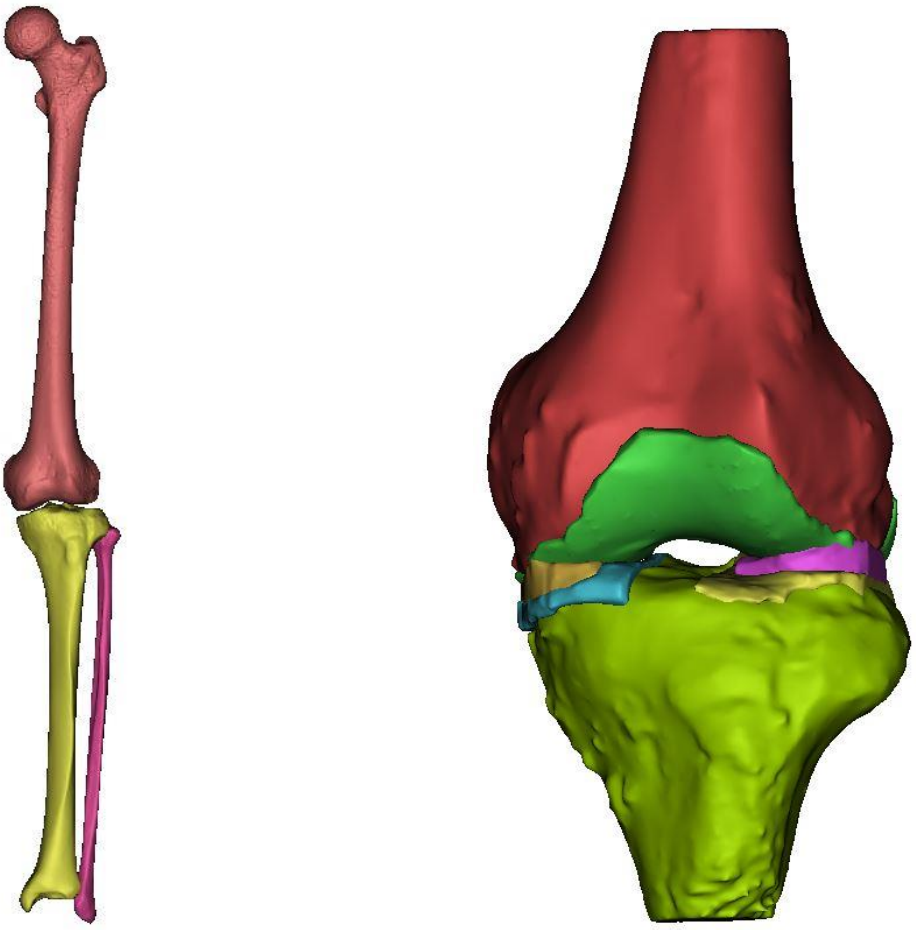

(a) (b)

Fig. 3-3 Reconstructed bone and soft tissue models (a): Reconstructed bone models based on CT images (b): Reconstructed bone and soft tissues models based on MR images

All the shell models optimized in 3-Matic software were imported into Geomagic DesignX to form solid models.

We notice that CT and MR image from different machines, each machine has the initial coordinate. The bony structure and soft tissues are in different coordinates due to the different initial machine coordinates. In this study, we need an intact and accurate knee model, thus, matching all the parts in the initial anatomical position is extremely important. We used N-point registration (Fig. 3-4) in 3-Matic software to match all the bones and soft tissue models.

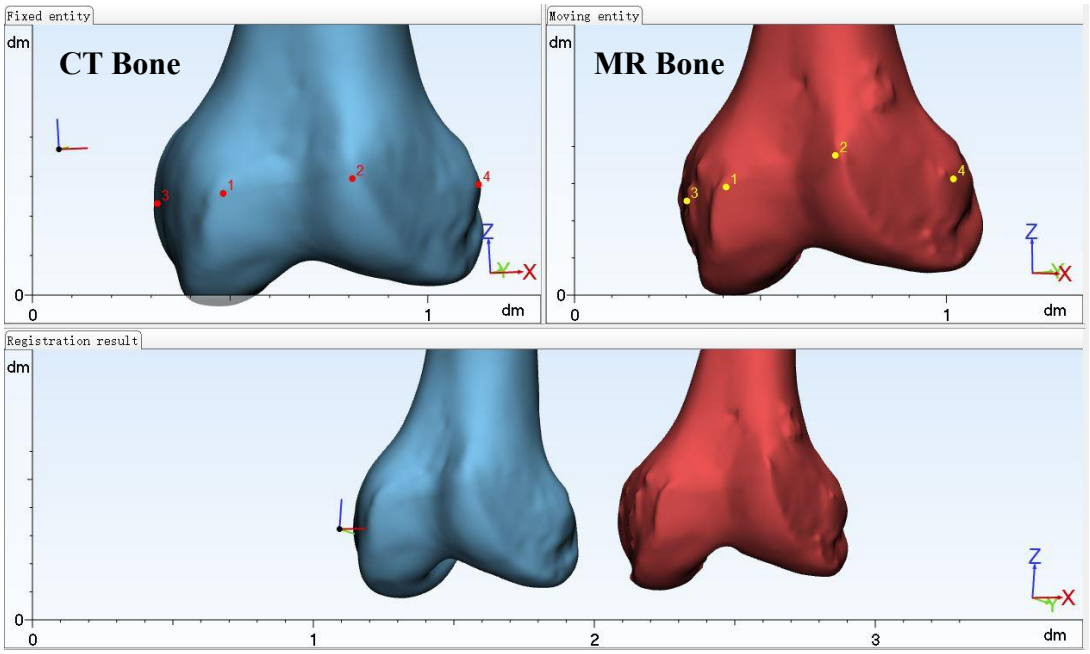

Fig. 3-4 Model registration

To solve the registration problem, we reconstructed femur, tibia, and fibula based on CT and MR, respectively. All the bone models were imported into 3-Matic software. The MR bone model (the bone model reconstructed based on MR images) was been fixed and defined several pairs of anatomical reference points on the CT bone model (the bone model reconstructed based on CT images) and MR bone model. The CT bone model was been moved to follow the defined reference points to match with the MR bone model. All the CT bone models were been matched with MR bone models in the model registration process.

The ideal netural alignmental knee is that the wight-bearing line cross the geometrical center of the tibial plateau, thus, the registrated bone model was imported into 3Dsmax software (version: 2018; Autodesk, Inc) to develop a netural alignmental knee model. A bending center point was defined on the fibula head and the bending region was selected on the tibia bone. The tibia bone was been bended a particular angle make the weight-bearing line cross the tibial plateau center (Fig. 3-5) and the Knee Joint Line Obliquity angle (knee joint line: the line from the medial side to the lateral side of the tibial plateau in coronal plane; KJLO angle: the angle between the joint and the line parallel to the ground) to be 0 degree (Fig.3-6).

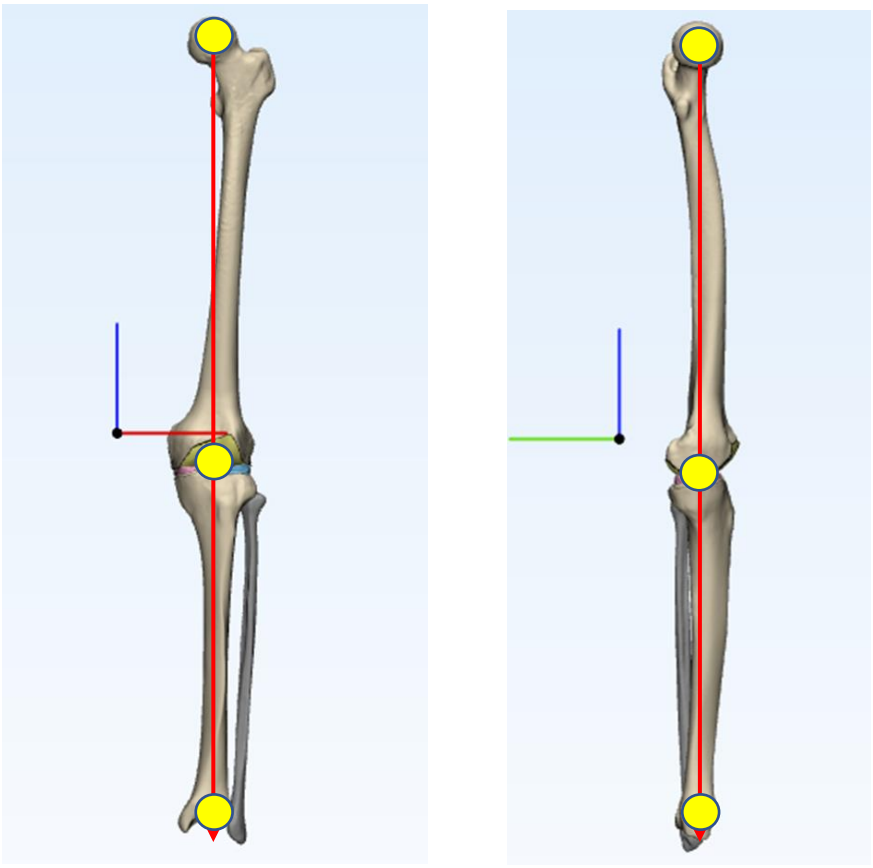

Fig. 3-5 Netural alignment model

All of the solid models obtained in 3-Matic and Geomagic DesignX were imported into Unigraphics NX (version: 8.0, Simens PLM Software, Torrance, CA, USA). The creation of an opening wedge on the medial side was performed under the guidance

of a clinician to simulate an HTO procedure. The hinge point defined in the safety zone of the fibula. The correction angle was designed at 10 degrees and a gap in the opening wedge was simulated by removing a wedge-shaped bone from the proximal tibia [20- 24].

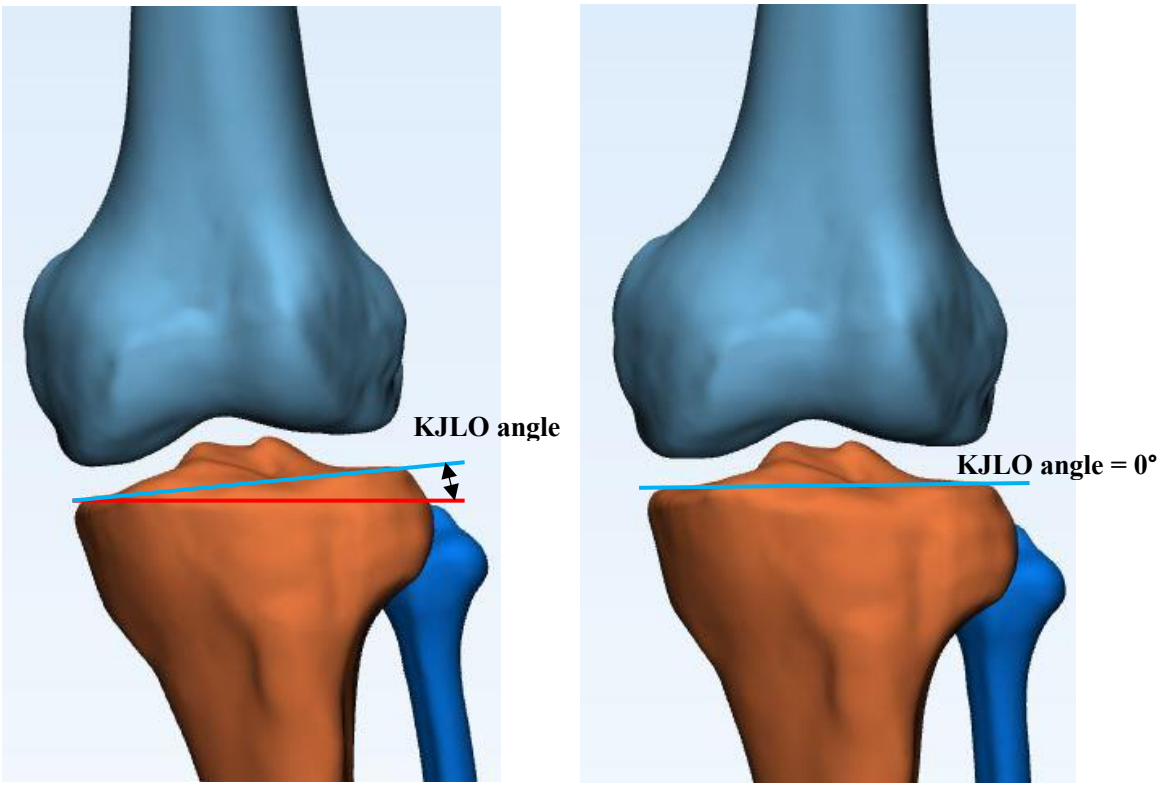

(a) (b)

Fig.3-6 KJLO angle (a): Definition KJLO angle (b): KJLO angle = 0 degree KJLO: knee joint obliquity. Blueline: the knee joint line. Redline: patella to the ground

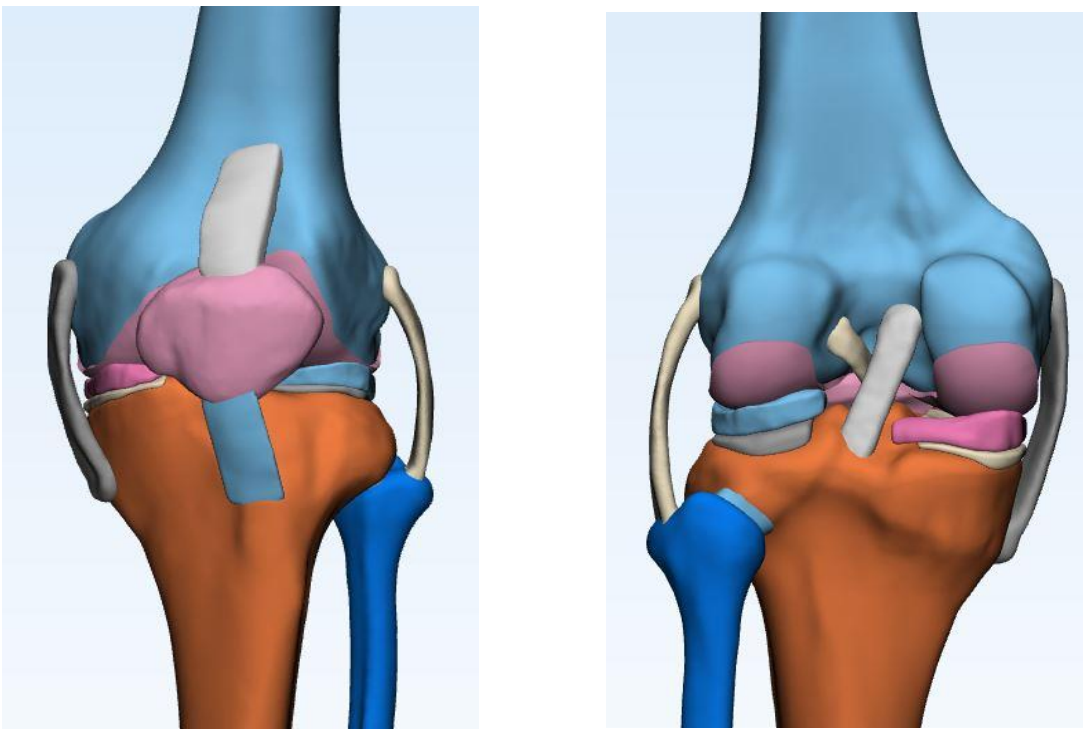

(a) (b)

Fig.3-7 Intact netural alignmental knee joint model (a): anterior view (b): posterior view

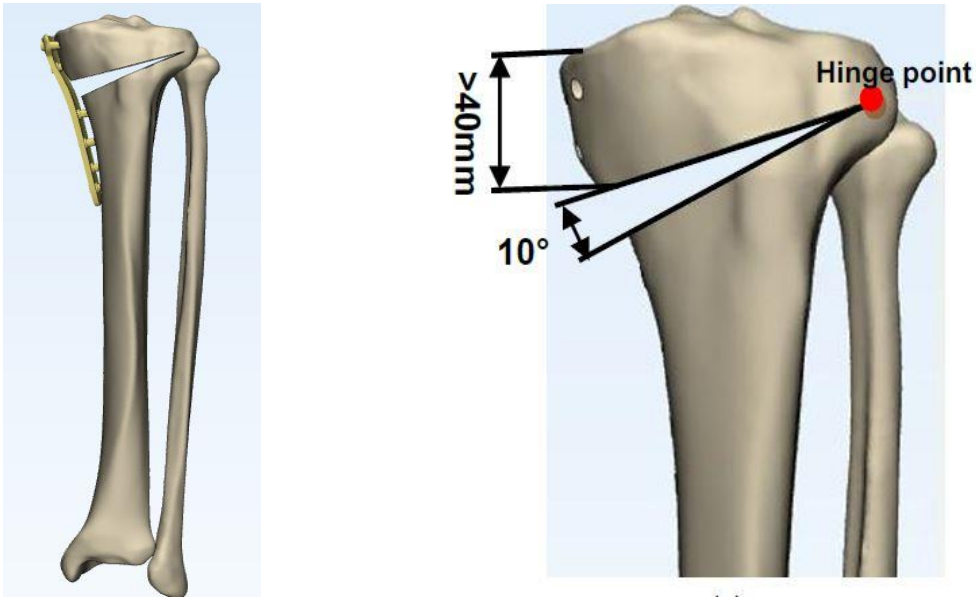

(a) (b)

Fig. 3-8 HTO model (a): After-HTO model fix with TomoFix plate (b): HTO opening wedge parameter

3.3 FE model

All of the solid models were imported into the Hypermesh software (version: 14.0; Altair Engineering, Troy, MI, USA) to generate FE mesh. The tetrahedral mesh was generated for all of the models due to the curved surface geometry structure of the bone, and the small size of the locking screws, soft tissues, and plate. The mesh sizes of the bone were 1 mm, soft tissues and screws, plate were 0.5 mm. The mesh quality check work was performed to confirm that the minimum mesh sizes of the bone were >0.5 mm and plate, screw and soft tissues were >0.3 mm.

Ultimately, 1,700,000 meshes were generated in total. The mesh model was imported into the ABAQUS (version: 2019; Dassault Systemes) software for finite element analysis.

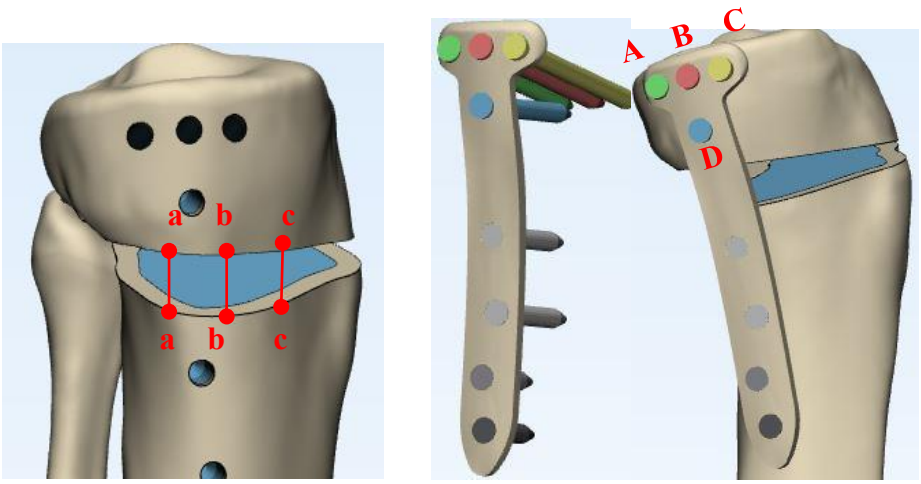

Fig. 3-9 (a): aa, bb, cc were defined to measure the interfragmentary micromotion (b): Tomofx system solid model (c): HTO model fixed with TomoFix system

3.3.1 Material properties

As introduced in the introduction part, there are 2 topics in this study, thus, 2 mesh models were generated. For the topic I (joint line obliquity) mesh model, the cancellous bone was not modeled. All of the bones were defined as linear elastic, homogenous and isotropic material with Young's modulus E = 8000 MPa and Poisson ration is 0.3 [58]. All the soft tissues (cartilage, ligament, meniscus, tendon) also were

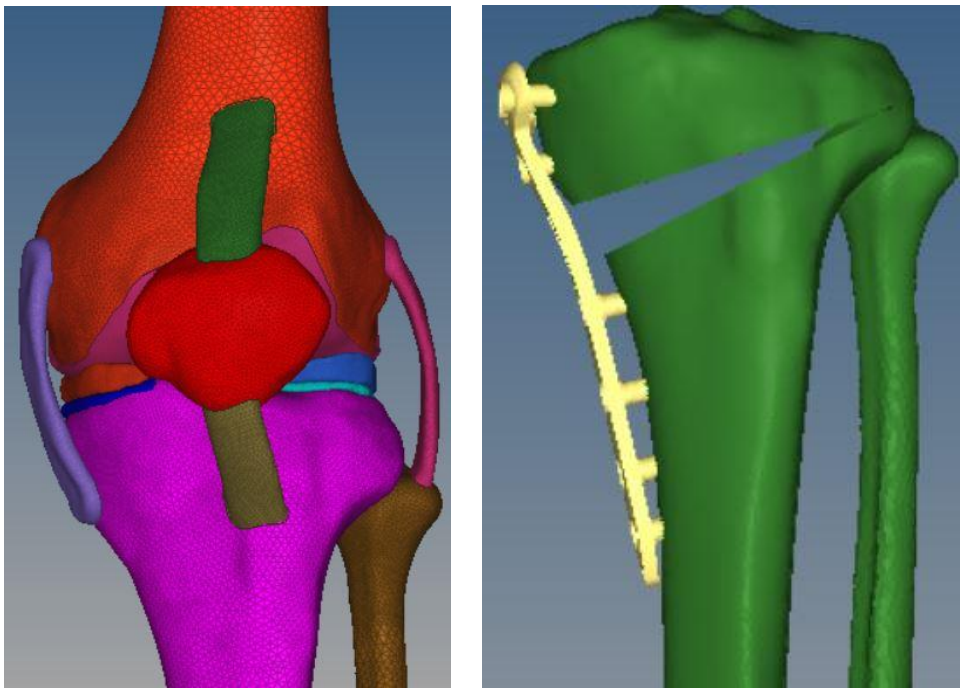

(a) (b)

Fig. 3-10 Mesh model used in this study (a): topic I mesh model (b): topic II mesh model

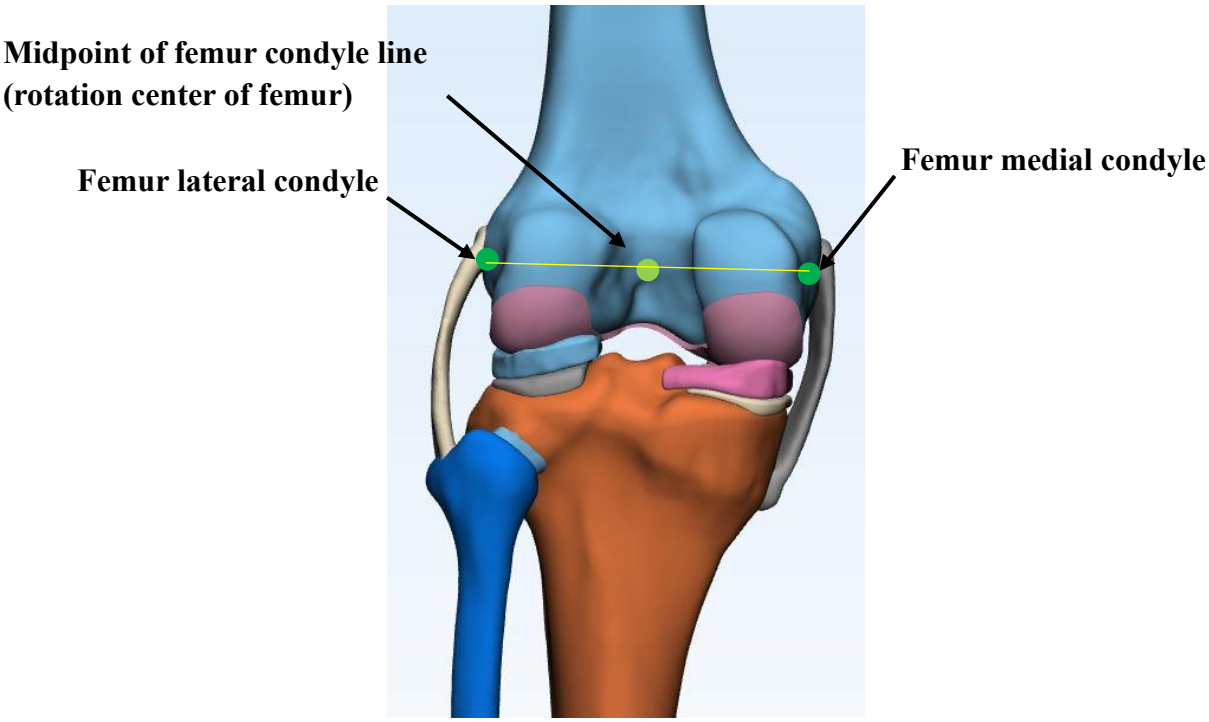

Fig. 3-11 Rotation center for femur

assumed to act as linear elastic, homogenous and isotropic. The Young's modulus of cartilage (femoral cartilage, lateral and medial tibial cartilage, tibia-fibula cartilage) is 15MPa and the Poisson ration is 0.475 refer to previous studies [58, 59]. The menisci are viscoelastic tissues, however, in short loading time during the stance phase of gait and a large viscoelastic time constant make it reasonable to assume meniscus as a single-phase, linear isotropic material with Young's modulus E = 59MPa and a Poisson ratio of 0.49 [18, 60]. The anterior cruciate ligament (ACL), posterior cruciate ligament (PCL), lateral collateral ligament (LCL), and medial collateral ligament (MCL) were assumed to act as linear elastic isotropic materials with a Poisson's ratio of 0.45 and Young's modulus of 300 MPa [61, 62]. In this study, we do not investigate the patella tendon, thus, we defined the same material property with ligament for patella tendon.

For the topic II (screw fixation stability) mesh model, The tibia bone (cortical bone and cancellous bone), screw and plate were defined to be linearly elastic, homogenous, and isotropic, respectively. Young's moduli of cortical bone and cancellous bone are 17 GPa and 5 GPa, respectively. Poisson's ratio is 0.33 [54, 55, 63]. The Tomofix plate and screw were made of titanium alloy for which Young's modulus is 110 GPa and the Poisson ratio is 0.3. The yield strength and tangent modulus in the plastic phase were defined as 800 MPa and 1250 MPa [54, 20], respectively. The bone graft was removed to simulate the worst condition for implant loading in the analysis.

3.3.2 Loading and boundary conditions

For the topic I, There are 2 load cases. An 1150 N vertical force was applied on the femur head for model validation [18]. A force of 2500 N, corresponding to 3.1 times the bodyweight of a person weighting 80kg was also applied, which is equivalent to the maximal axial force during the gain cycle [43, 53, 64]. The midpoint of femur condyle line was defined as the femur rotation center, the line that crosses this point and perpendicular to the coronal plane as the femur rotation axis. The femur was rotated around the rotation axis 1.5 degrees, 2.5 degrees, 3.5 degrees equals to 2

degrees, 4 degrees, 6 degrees varus when the 2500 N force was applied during the Abaqus analysis.

Meniscus-femoral cartilage, meniscus-tibial cartilage were defined as the frictionless surface to surface contact to mimic the joint lubrication [65]. Attachments between soft tissues (cartilage, ligament, tendon)and bones were achieved by defining tie contact. The anterior and posterior horn of meniscus, tibia, and fibula were constrained in 6 degrees of freedom for all of the analysis, the femur was just allow move follow the vertical force direction.

For topic II, vertical forces of 1000 N and 500 N were applied to the tibial plateau to measure the micromotion. According to a previous study, a 1400-N knee physiological transfer load was assumed, which is a vertical load on the tibial plateau with 40% on the medial side and 60% on the lateral side [66] when one locking screw is missing (locking screw A, B, C, D). The tie contact was defined for all contact surfaces (cortical bone-cancellous bone, bone-screw, screw-plate) to simulate the bond interaction [53-55, 67]. The locking screw threads are disregarded for numerical simplification. and the distal end of the tibia was set to 0 in all degrees of freedom. The equivalent stress (von Mises stress) was the index to evaluate the stress on the locking screw, plate, and bone. The opening wedge micromotion changes of edges aa, bb, and cc as the index of TomoFix system fixation stability [54,55].

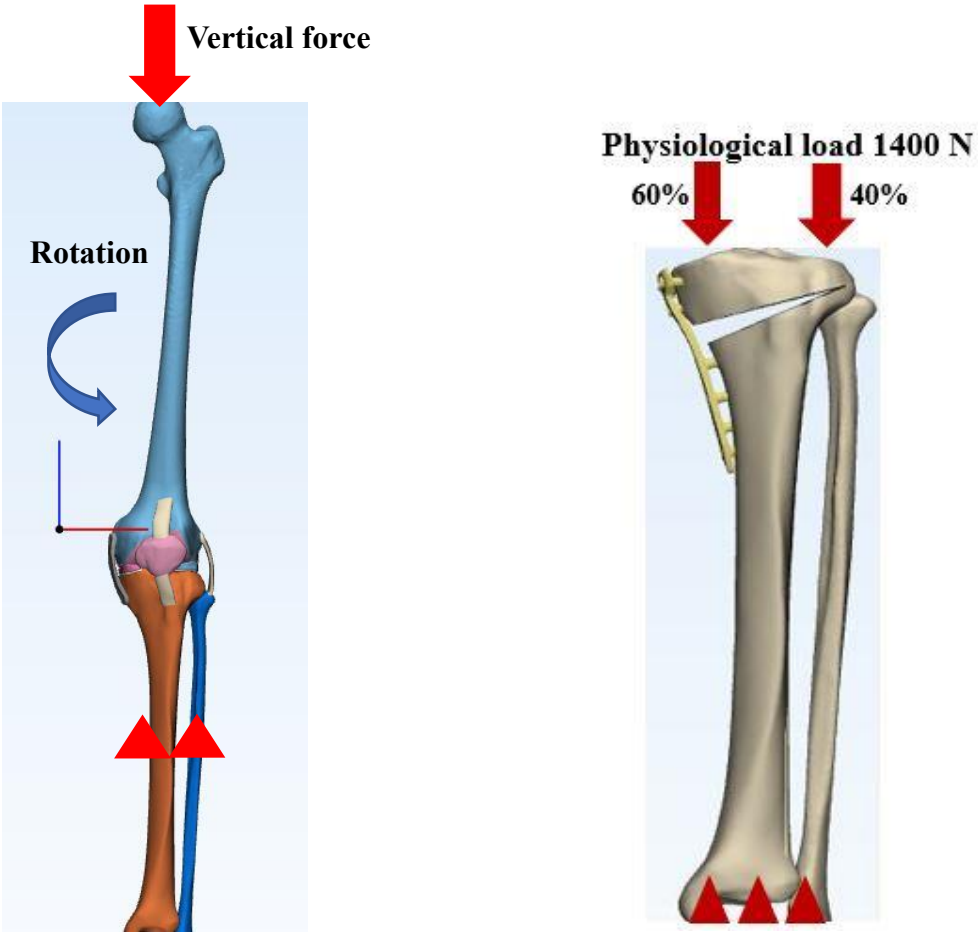

(a) (b)

Fig. 3-12 Load and boundary condition (a): topic I load and boundary condition (b): topic II boundary condition

Chapter 4 Results and discussion

4.1 Model validation

In this study, we developed an intact 3D lower limb model of the healthy human. This model includes four complete bones (fumer, tibia, fibula, patella), four main ligaments (ACL, PCL, MCL, LCL), two patella tendons, and knee joint cartilages.

A compressive load of 1150 N was applied on the femur head refer to a previous study [18, 69]. Based on the FEA results, the peak contact pressure occurred at the posterior region of the medial meniscus and anterior region of the lateral meniscus with a value of 3.33 and 3.75, respectively. This corresponded to the contact zones between the femur and menisci were very similar to the study results obtained with the experimental method by Walker and Erkman [68]. Pena et al found the highest contact pressure in the same region of the meniscus with a value of 3.15 MPa and 3.68 MPa [18], Dong et al also get a similar result in the same region with the value of 3.55 MPa and 3.24 MPa [69]. Bendjaballah et al. considered that the compressive stress in the meniscus varied from -1 to -4 MPa for a healthy knee under a compressive load of 1300 N [70]. Similar results were obtained in this study, the compressive stress in the lateral meniscus is -3.83 MPa and -2.17 MPa in the medial meniscus. Pena et al. found the compressive stress in the lateral meniscus and medial meniscus are -3.82MPa and -2.15 MPa, respectively. Pena et al's study results indicated that the compressive stress in the medial and lateral side of femur cartilage is -2.68 MPa and -3.11 MPa. Similar results were obtained in this study, the compressive stress in the medial side is -3.0 MPa and -3.83 MPa in the lateral side of femur cartilage. They also measured the compressive stress in lateral and medial tibia cartilage with a value of -1.76 MPa and -2.19 MPa, respectively. Based on our FEA results, the compressive stress in the lateral tibia cartilage is -2.15 MPa and -2.6 MPa in medial tibia cartilage, this slight deviation may due to the individual and model difference. Fukubayashi and Kurosawa measured the contact area of the knee joint [71]. The contact area of the medial plateau of the knee joint was 300 ± 80 mm^2 under an axial compressive load of 1000 N. Our calculation showed that the contact area of the medial plateau was 310 mm^2 under 1150 N, the similar was obtained by Pena et

al with a contact area of 359 mm^2 at the medial plateau under a vertical load of 1150 N.

Pena et al's study also showed that the menisci transferred about 75% of the total axial load, in this study, the menisci transferred 76% of the total axial load based on our calculation. Based on the validation results, on an overall basis, it could be confirmed the ability of our FE model to produce convincing results.

For the HTO FE model validation, 500 (corresponding to partial load bearing of the leg) and 1000 N (corresponding to an almost full-load bearing of the leg) vertical forces were applied on the tibial plateau [72]. The maximum interfragmentary movements of the opening wedge were measured, and the results were compared to those of Gotz Roderer et al. and Yen-Nien Chen et al. [72, 20]. The interfragmentary movement of this FE model is similar to that found in previous studies (Fig. 4-1). The interfragmentary movement difference between this FE model and Gotz Roderer et al.'s study is 0.02 mm (under 500 N and 1000 N). The results difference between this model and Yen-Nien Chen et al.'s study is 0.01 mm and 0.02 mm under 500 N and 1000 N, respectively.

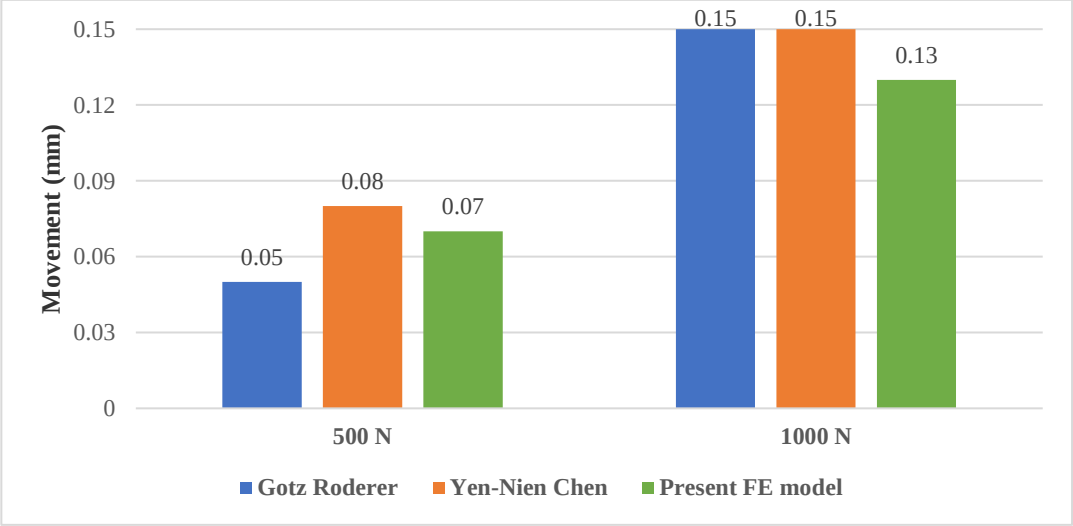

Fig. 4-1 Comparison of interfragmentary movement of the opening wedge

The interfragmentary movement of the present FE model was consistent with that of previous studies in which the deviation was <0.02. This finding may have been

caused by model geometrical differences, individual differences, or different correction angles. However, overall, the consistency between the validation result and those of previous studies confirms the ability of the present model to produce convincing results.

4.2 Results and discussion

4.2.1 Topic I

In chapter 3, we applied the same load and boundary condition with a previous study to the model. Many indexes were compared with the results of previous studies. The model validation results showed considerable consistency between our results and literature, confirmed the ability of our model to produce reasonable results.

The midpoint of the femur condyle line as the rotation center, the line cross this point and perpendicular to the coronal plane as the femur rotation axis. The femur bone was rotated 1.5 degrees, 2.5 degrees, 3.5 degrees equal to 2 degrees, 4 degrees, 6 degrees varus deformity. A vertical load of 2500 N was applied to the femur head. The Von-Mises stress, contact pressure, compressive stress, and shear stress on soft tissues as the indexes to evaluate biomechanical environment change between the varus knee and After-HTO knee. In this topic, the 6 DOFs (degrees of freedom) of the tibia and fibula bone were constrained and we did not investigate the plate and screws, thus, the opening-wedge was not be created, the TomoFix plate also did not apply. The normal knee model was used as the after-HTO model.

1. Meniscus

Meniscus located in the joint cavity, contact with femur cartilage, and tibia cartilage. Meniscus always is compressed when the joint space decrease.

As shown in Fig. 4-2, the stress and contact pressure on the lateral side were unchanged when the varus angle increase. However, the contact pressure was decreased by 32% (from 8.4MPa to 5.7MPa)compared with the normal knee. This change may due to the increased contact area when the varus deformity occurred.

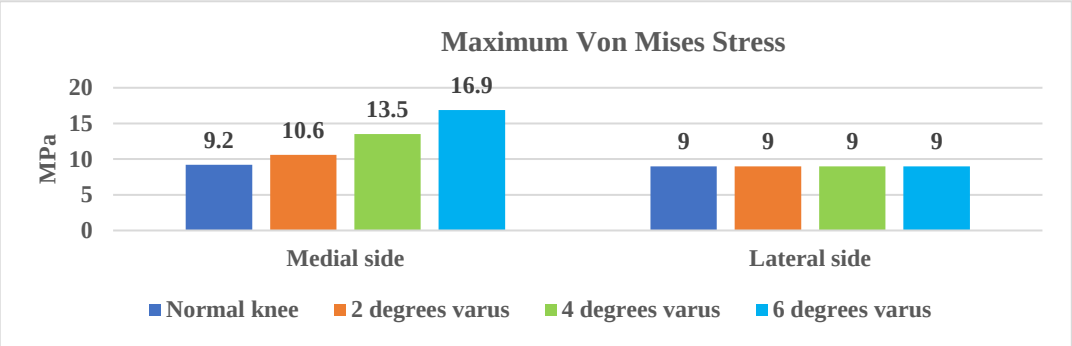

(a)

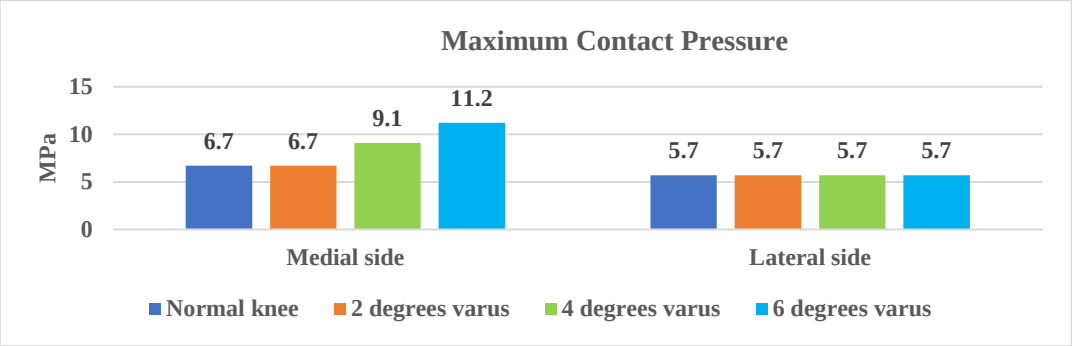

(b)

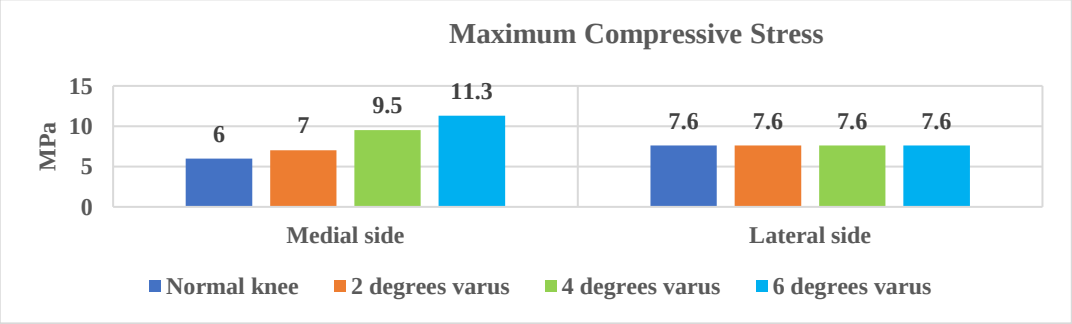

(c)

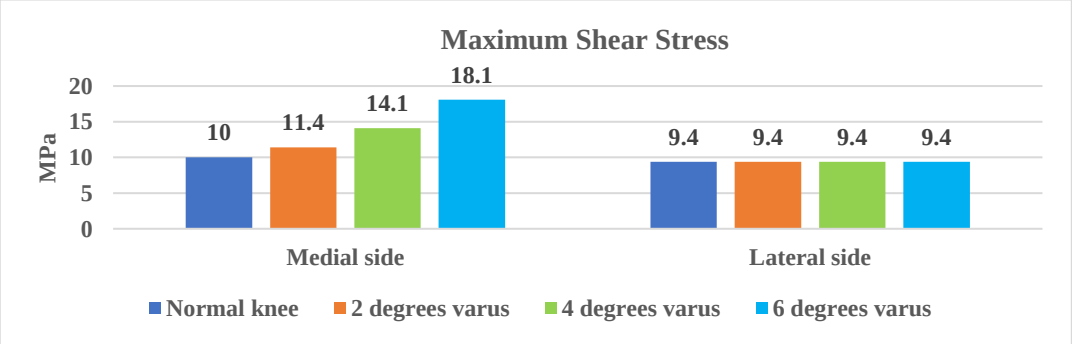

(d)

Fig. 4-2 Meniscus indexes comparison between normal and varus knee (a): Von Mises stress (b): contact pressure (c): compressive stress (d): shear stress

The stress and contact pressure on the medial and lateral side were slightly different for a normal knee, however, this balance was broken with the increase of varus angle. Compare with the normal knee, the von mises stress on medial meniscus was increased by 15.2%, 46.7%, 83.7% when the varus angle is 2 degrees, 4 degrees, 6degrees, respectively. The contact pressure on medial meniscus did not increase when the varus angle was 2 degrees, this may due to the contact area between medial meniscus and cartilages did not change when the knee with a small angle varus deformity. However, the contact pressure on medial meniscus was substantially increased by 35.8% and 67.2% when the varus angle increased to 4 and 6 degrees.

The compressive stress was occurred by the contact force in the direction perpendicular to the contact surface. The contact pressure on medial meniscus was unchanged but the compressive stress was increased by 16.7% when varus angle was 2 degrees. The compressive stress was increased by 58.3% when the varus angle increased to 4 degrees and it increased 88.3% when the varus was 6 degrees. The shear stress on medial meniscus was increased by 14%, 41%, and 81% when the varus angle was 2 degrees, 4 degrees, and 6 degrees, respectively.

Based on our FE analysis results, all the indexes on medial meniscus were significantly increased when the knee with a varus angle, the stress and contact pressure on the lateral meniscus almost unchanged. The biomechanical balance of knee joint was broken by varus deformity. Various clinical studies have proved the relationship between knee OA and meniscus tear [73-75]. They supposed that changes resulted by meniscus tear in contact stress led to this relationship. This is consistent with our FE analysis results, varus deformity led to the increase of stress and contact pressure, these changes led to meniscus tear thus lead to OA. On the other side, OA makes the meniscus tear progress accelerating.

In other words, as mentioned, the normal knee was used as the after-HTO knee. The comparative result indicated that the stress and contact pressure on medial meniscus were decreased, the knee from an unbalanced biomechanical environment to be balanced.

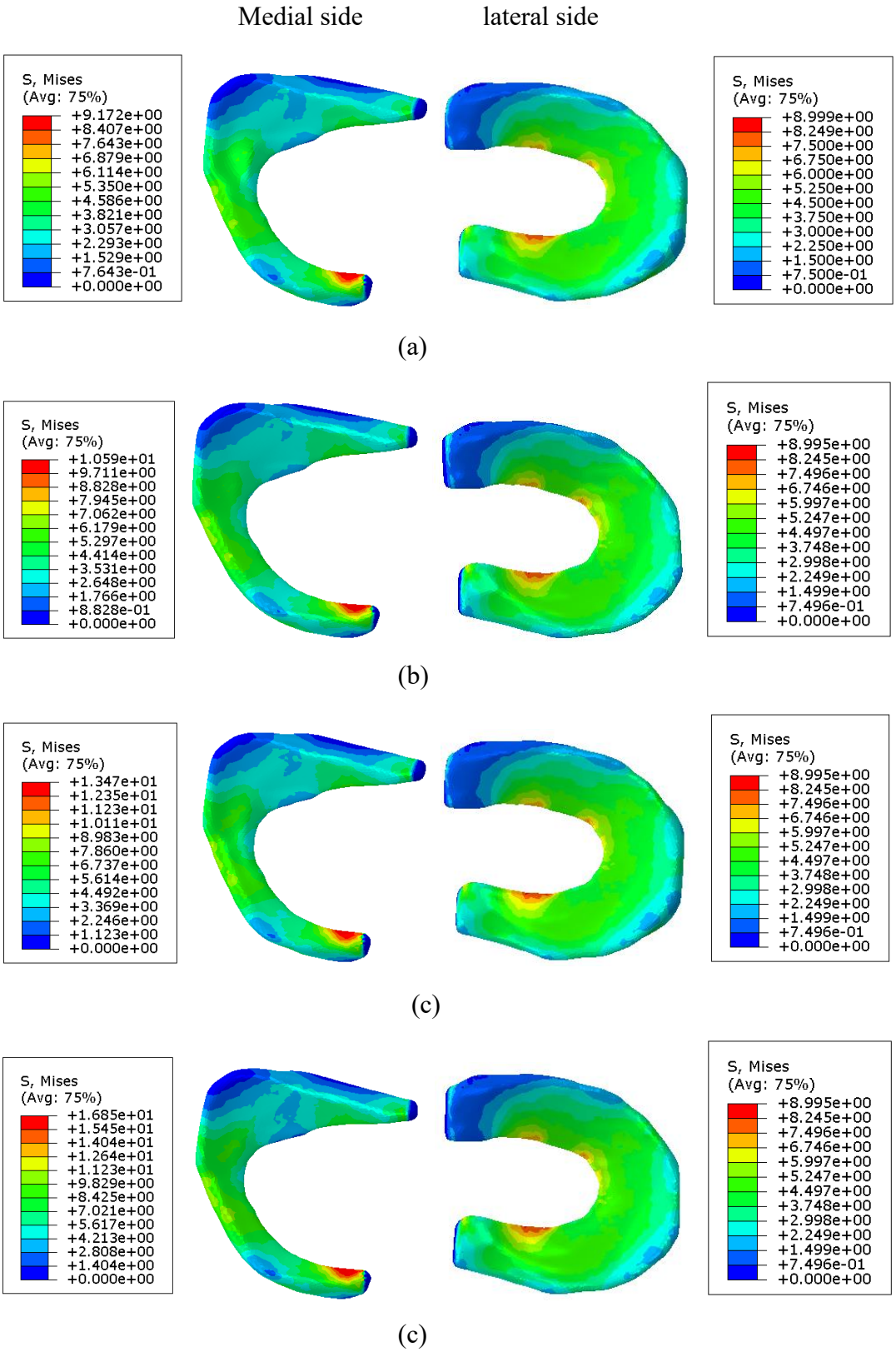

Fig. 4-3 Von Mises stress distribution on meniscus (a): normal knee (b): 2 degres varus knee (c): 4 degrees varus knee (d): 6 degrees varus knee

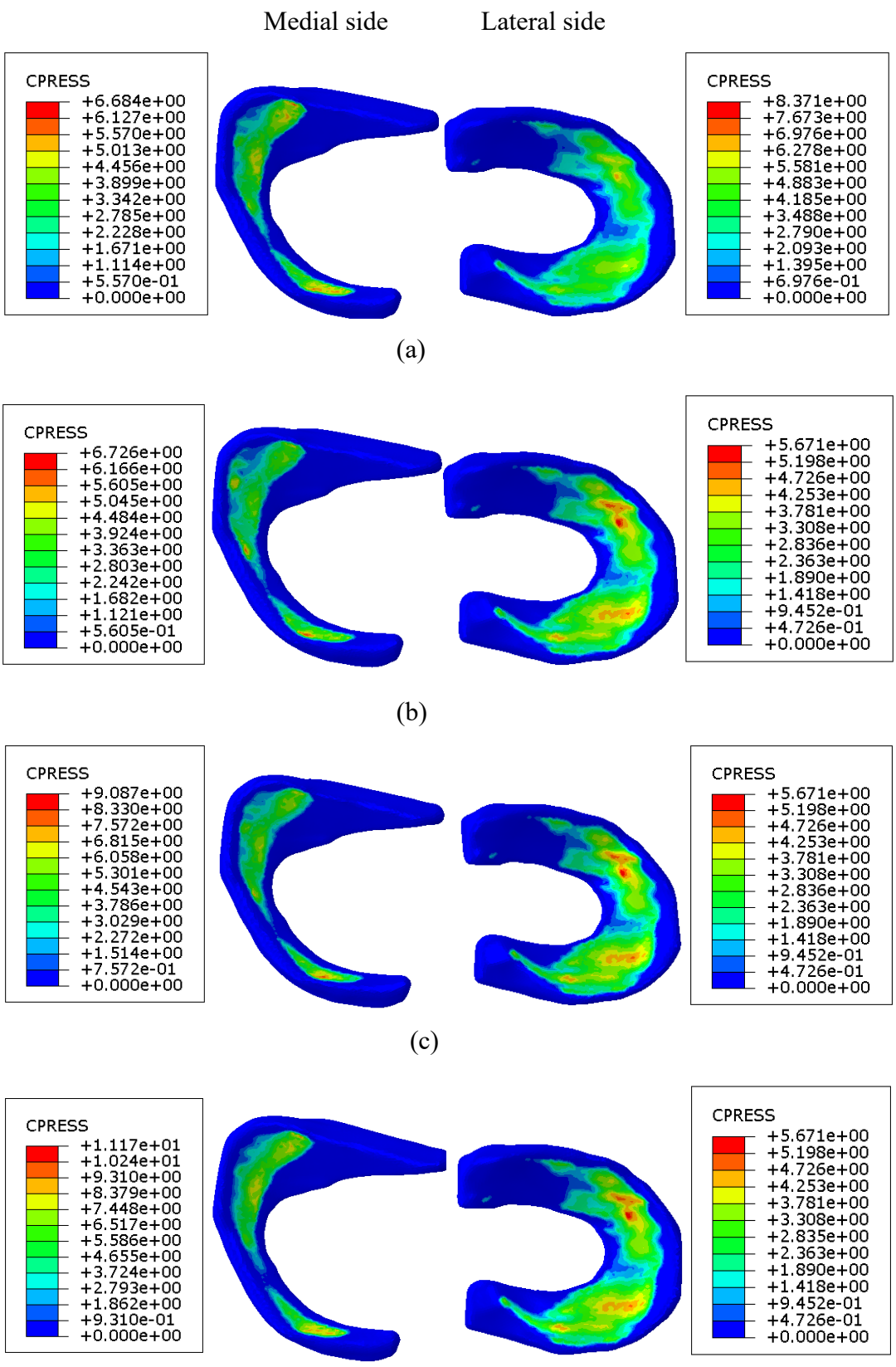

Fig. 4-4 Contact pressure distribution on meniscus (a): normal knee (b): 2 degrees varus knee (c): 4 degrees varus knee (d): 6 degrees varus knee

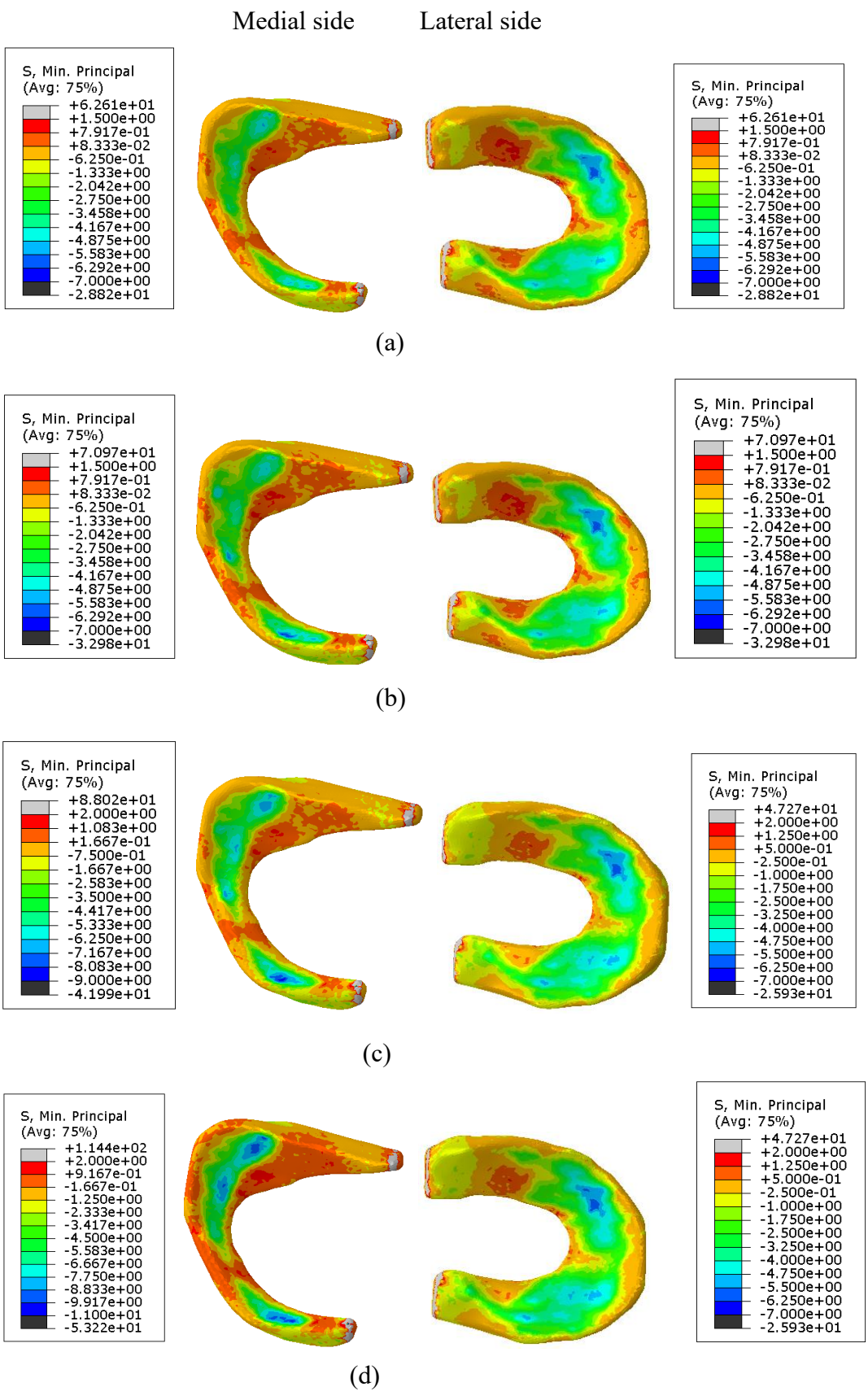

Fig. 4-5 Pressive stress distribution on meniscus (a): normal knee (b): 2 degrees varus knee (c): 4 degrees varus knee (d): 6 degrees varus knee

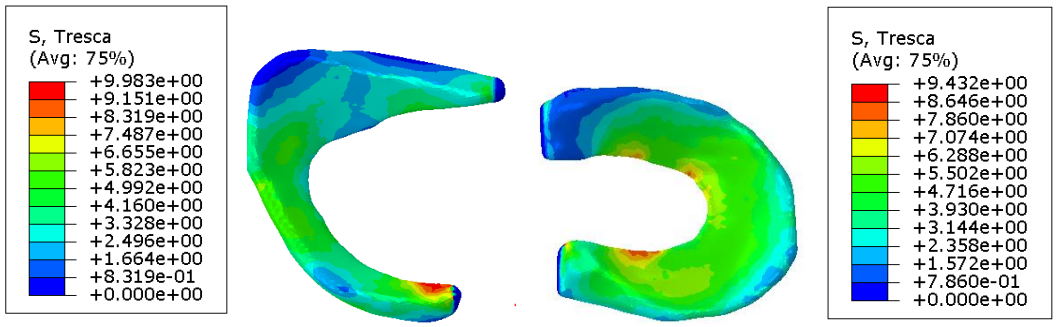

(a)

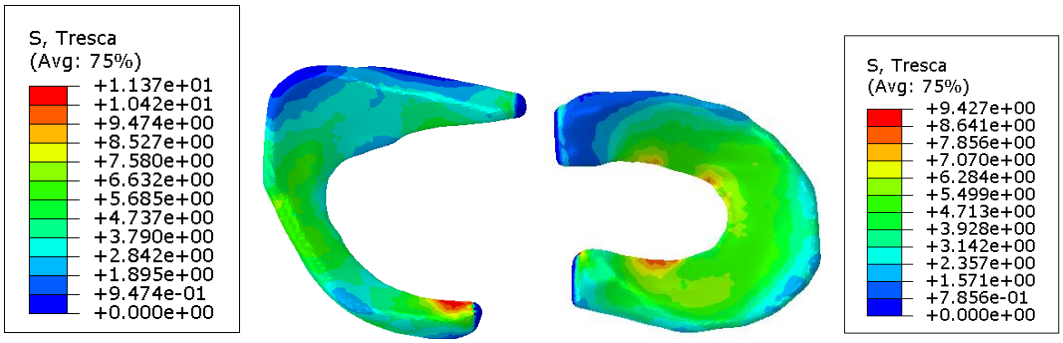

(b)

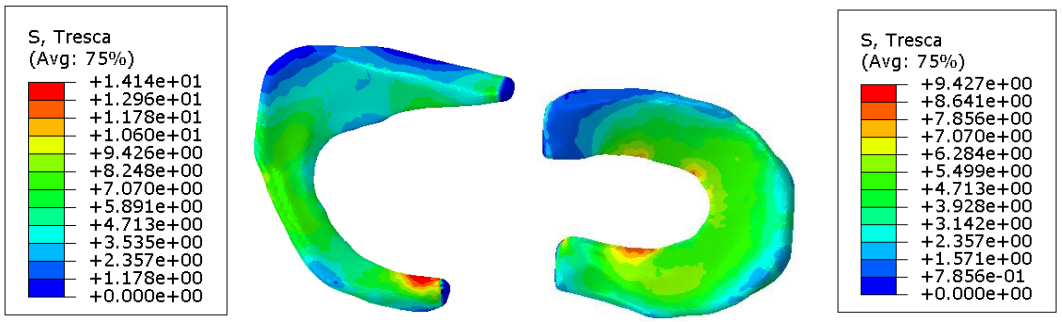

(c)

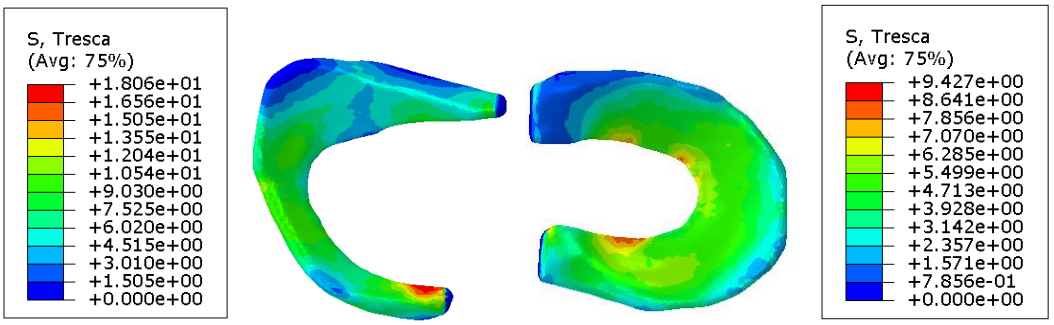

(d)

Fig. 4-6 Shear stress distribution on meniscus (a): normal knee (b): 2 degrees varus knee (c): 4 degrees varus knee (d): 6 degrees varus knee

2. Femur cartilage

The femur cartilage attached to the femur bone and contact with the meniscus when the load was applied on the femur head. In this study, we applied a vertical load of 2500 N equals to 3.1 times body-weight (80 Kg), in this extreme condition, the femur cartilage compress the meniscus more and the contact area with meniscus and tibia cartilage were increased.

As shown in Fig.4-7, for the normal knee, all the indexes on both sides were almost the same. The stress on the lateral side was just slightly changed, the compressive stress on the lateral side was decreased following the increase of varus angle but the compressive stress on the medial side was increased 50.6%, 96%, and 140% when the varus angle increased to 2 degrees, 4 degrees, 6 degrees, respectively. This phenomenon shows that the compressive stress was transferred from the lateral side to the medial side when the knee with a varus angle, besides, the compressive stress increased more when the varus angle became bigger.

The von mises stress on the medial side was increased by 12.5% when the varus was 2 degrees compare to the normal knee. Following the increase in varus angle, the von mise stress on the medial side was increased by 58.3% and 95.8% when the varus angle was 4 and 6 degrees. The contact pressure on the medial side was increased by 17.6%, 52.9%, and 76.5% when the varus angle increased from 0 degrees to 2 degrees, 4 degrees, 6 degrees. The shear was just increased by 10.7% when the varus is 2 degrees, it was increased by 53.6%, 89.3% when the varus angle increased to 4 degrees and 6 degrees.

From the contour figures (Fig,4-8 - Fig4-11), we can see that the maximum value occurred location all transferred from the lateral side to the medial side. For the normal knee, all the stress on the medial side and the lateral side were almost the same. Lee et al. proposed that increased contact stress plays a major role in the degenerative changes for knee cartilages [76]. Our calculations indicated that the stress on the medial side was significantly increased. Based on our results, we believe that increased stress could be the risk factor of the cartilage tear and after HTO the stress distribution became balanced on both sides.

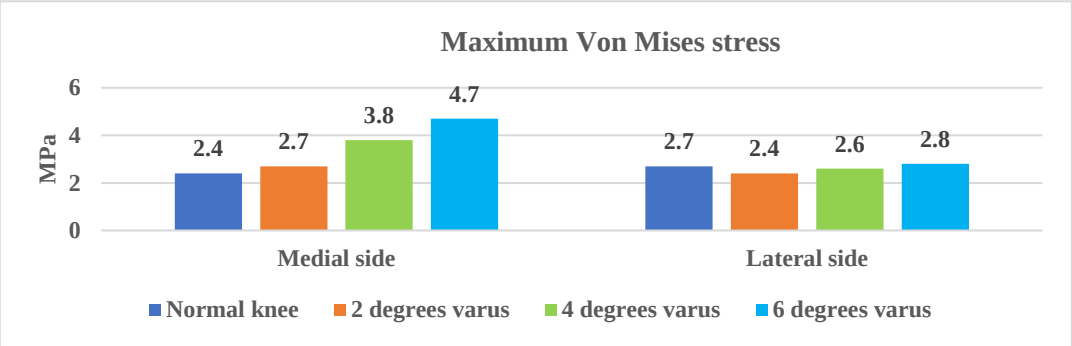

(a)

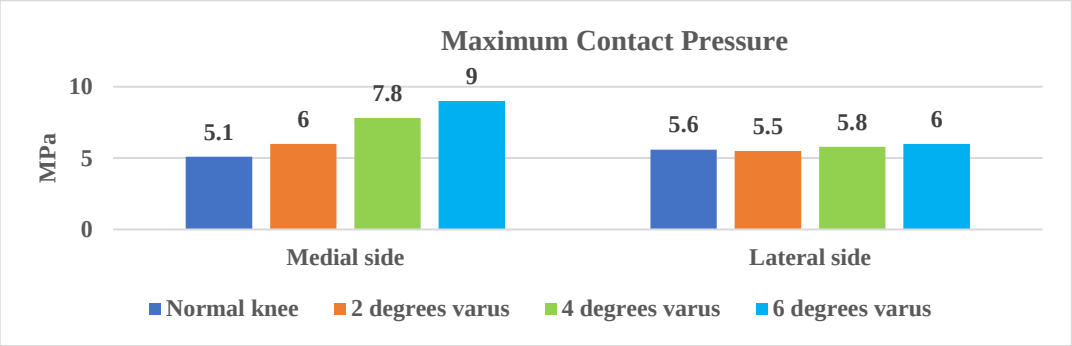

(b)

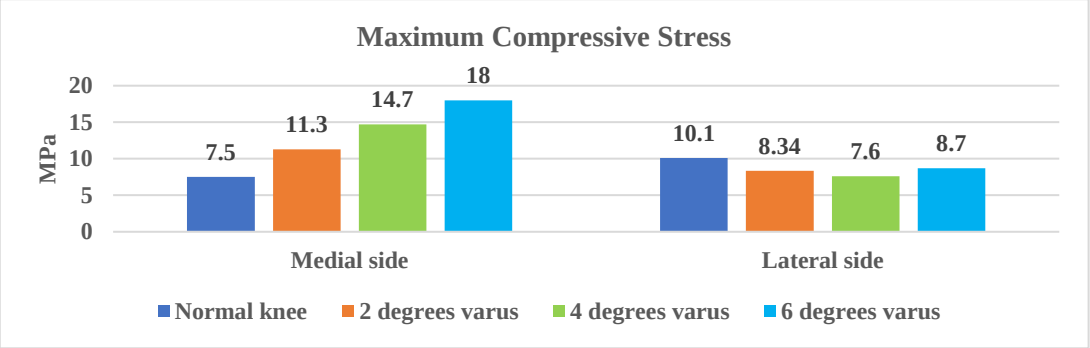

(c)

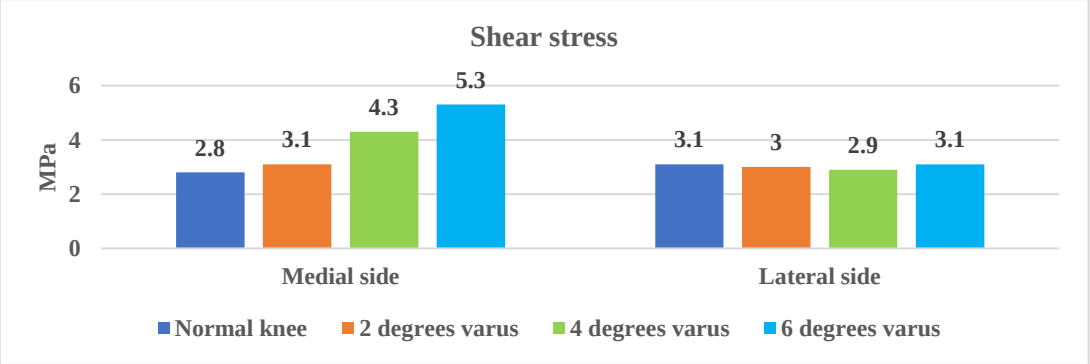

(d)

Fig. 4-7 Femur cartilage indexes comparison between normal and varus knee (a): Von Mises stress (b): contact pressure (c): compressive stress (d): shear stress

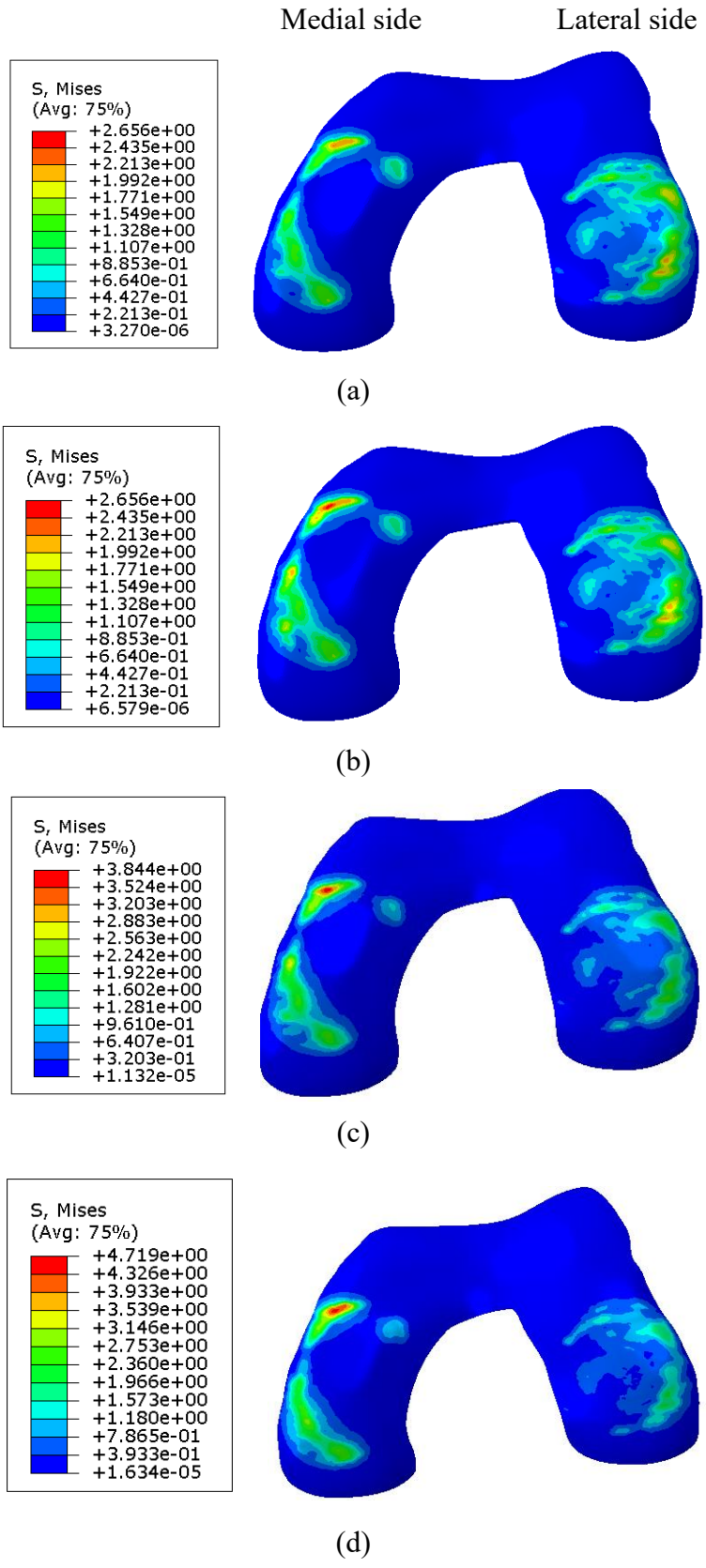

Fig. 4-8 Von Mises stress distribution on femur cartilage (a): normal knee (b): 2 degrees varus knee (c): 4 degrees varus knee (d): 6 degrees varus knee

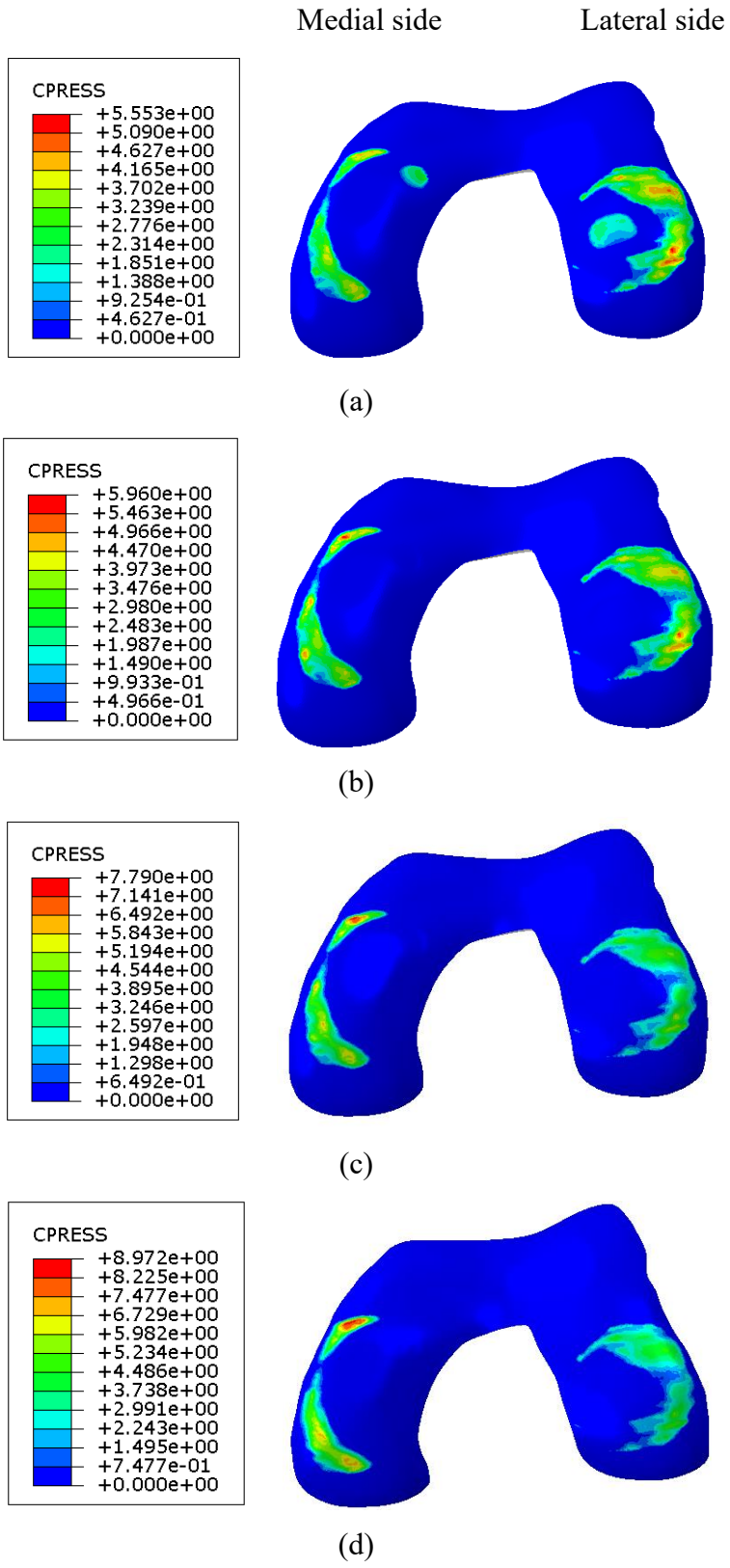

Fig. 4-9 Contact pressure distribution on femur cartilage (a): normal knee (b): 2 degrees varus knee (c): 4 degrees varus knee (d): 6 degrees varus knee

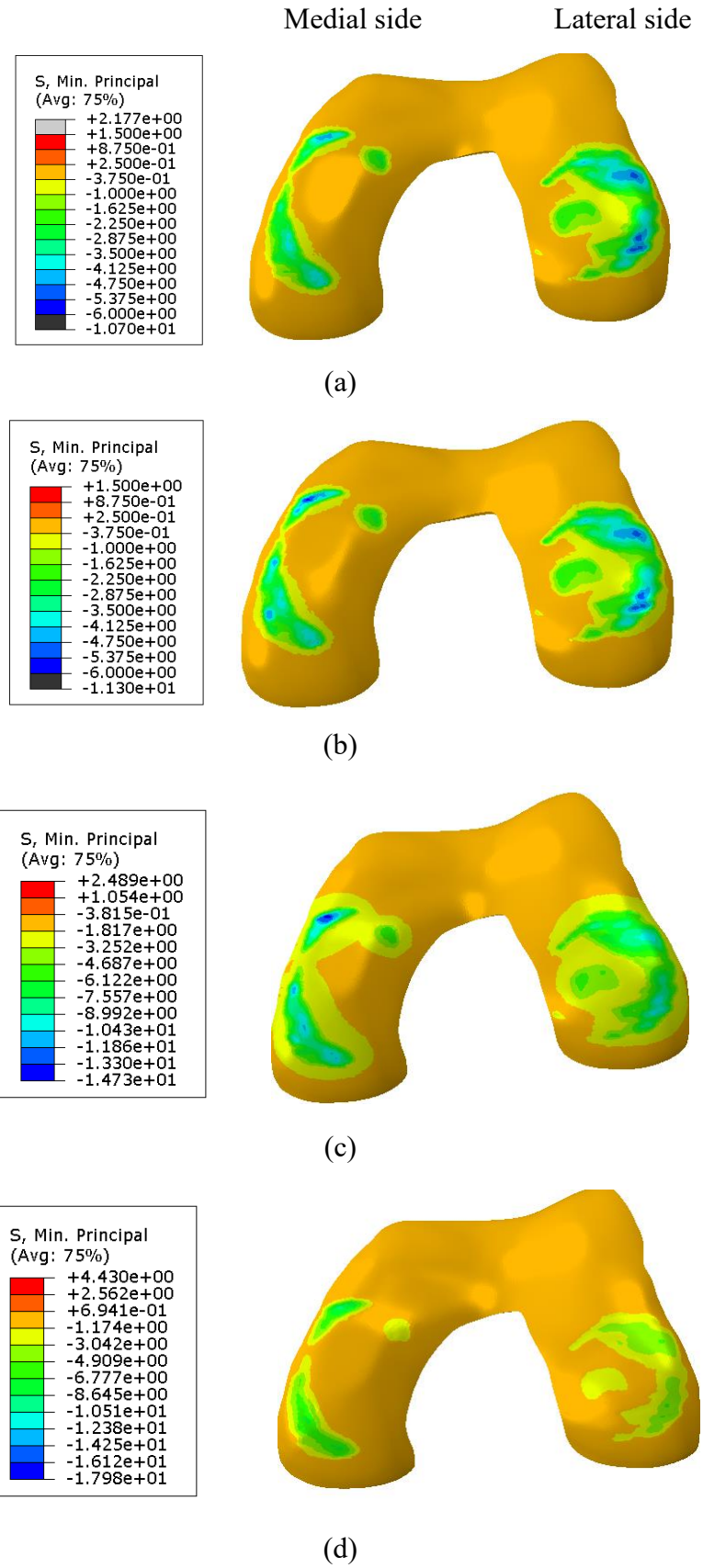

Fig. 4-10 Compressive stress distribution on femur cartilage (a): normal knee (b): 2 degrees varus knee (c): 4 degrees varus knee (d): 6 degrees varus knee

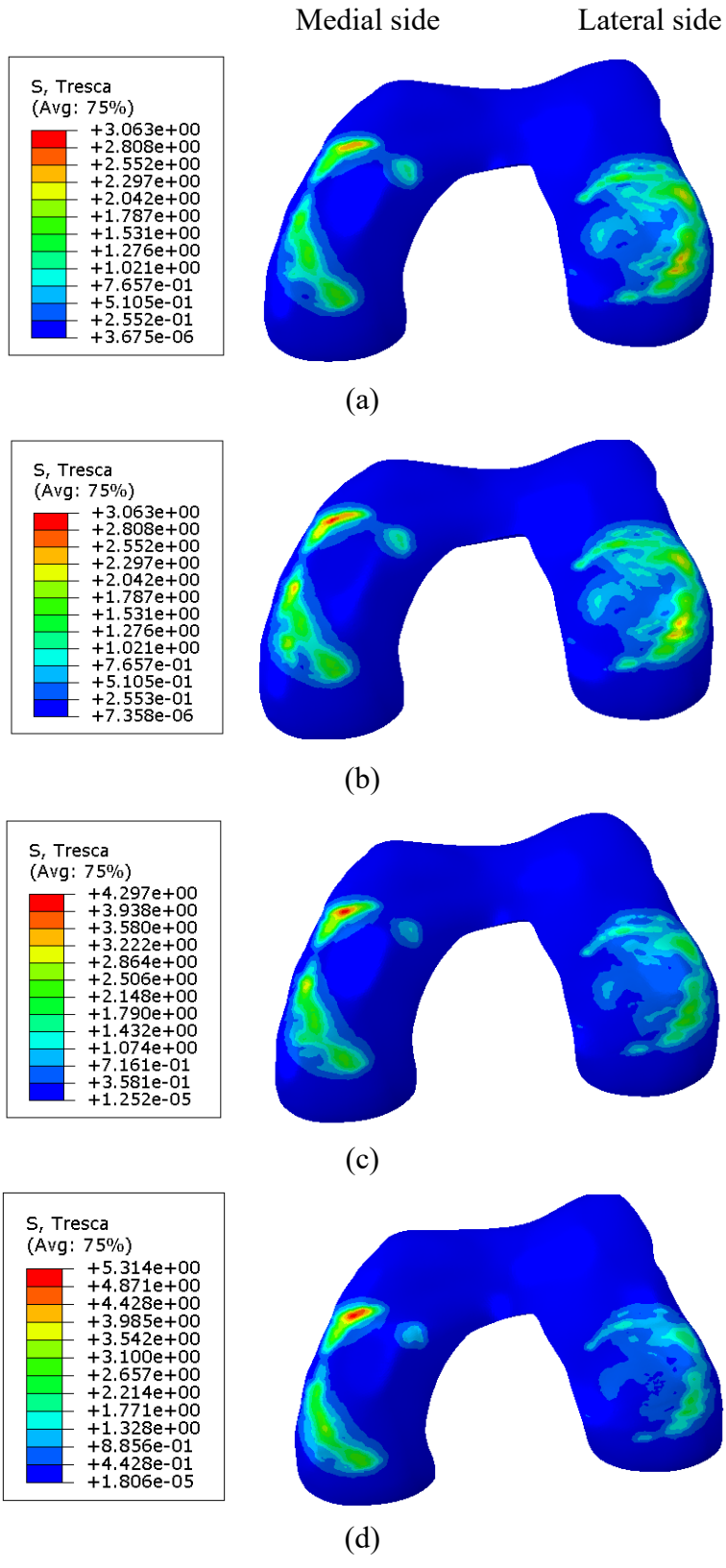

Fig. 4-11 Shear stress distribution on femur cartilage (a): normal knee (b): 2 degrees varus knee (c): 4 degrees varus knee (d): 6 degrees

3. Tibia cartilage

Tibia cartilage was attached to the tibia plateau, contact with the bottom surface of the meniscus. The cartilage will contact with the femur cartilage when the femur bears a huge load. Tibia cartilage bears all the load transfer from the meniscus and femur cartilage. OA is often accompanied by cartilage damage. The long-term excessive load will cause cartilage degeneration and cartilage injury [76].

As shown in Fig.4-12, all the indexes on lateral tibia cartilage remained unchanged under different varus angle deformities. Compared to the normal knee, all the stress and contact pressure on medial tibia cartilage were increased differently. The compressive stress on the medial tibia cartilage increased the most with the value of 15.6%, 56.7%, 97.8% when the varus angle is 2 degrees, 4 degrees, 6 degrees. This may occur by the decrease in medial side joint space. The von mises stress on medial tibia cartilage was increased 12.5% when the varus angle is 2 degrees and it increased 57.5%, 87.5% when the varus angle is 4 and 6 degrees, respectively. The shear stress on medial tibia cartilage was increased the most compared to that on the medial meniscus and femur cartilage medial side. The shear stress on medial tibia cartilage increased by 14.6%, 58.3%, 85.4% when the varus angle is 2 degrees, 4 degrees, and 6 degrees.

For the normal, based on our calculation, we found that the von mises stress, contact pressure, and shear stress on the lateral side and medial side were with a small difference. This may be caused by individual differences or modeling errors. On the whole, the stress and contact pressure distribution on both sides were uniform, the knee was in a balanced biomechanical environment.

Based on our FE analysis results, overall, all the stress and contact pressure were substantially increased following the increase in varus angle. Refer to the previous study's results[76] and our calculation, we propose that the increased stress and contact pressure may lead to cartilage tear and degeneration.

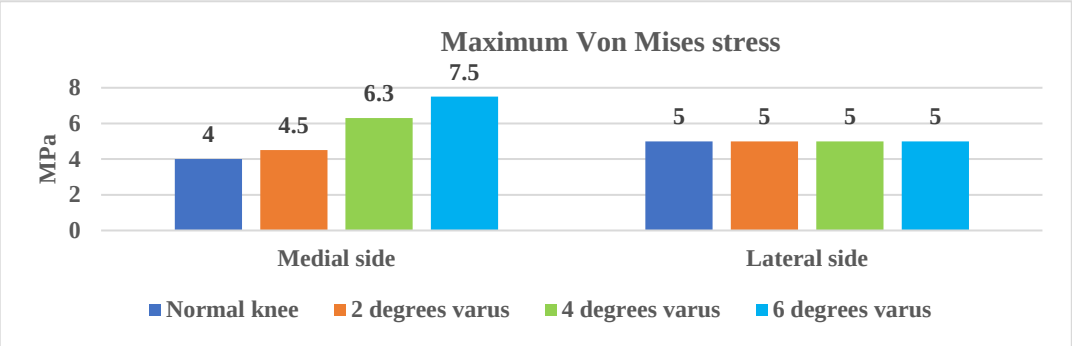

(a)

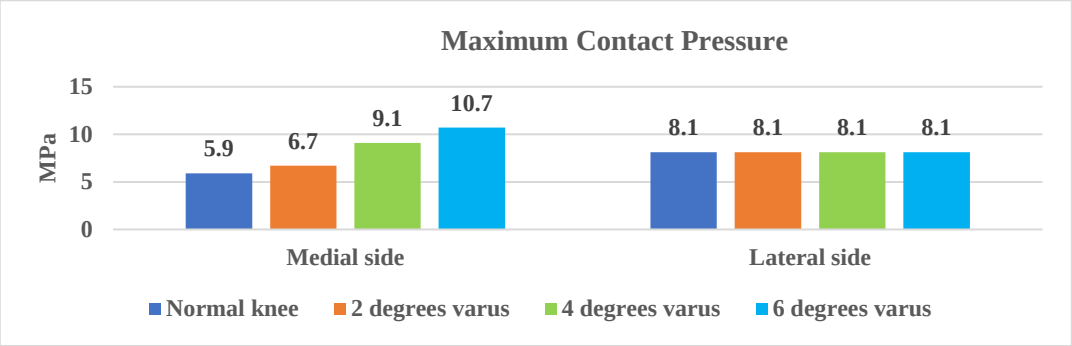

(b)

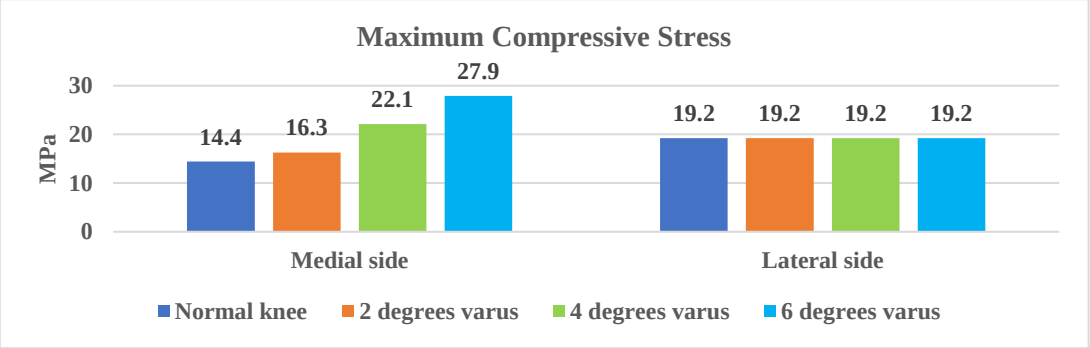

(c)

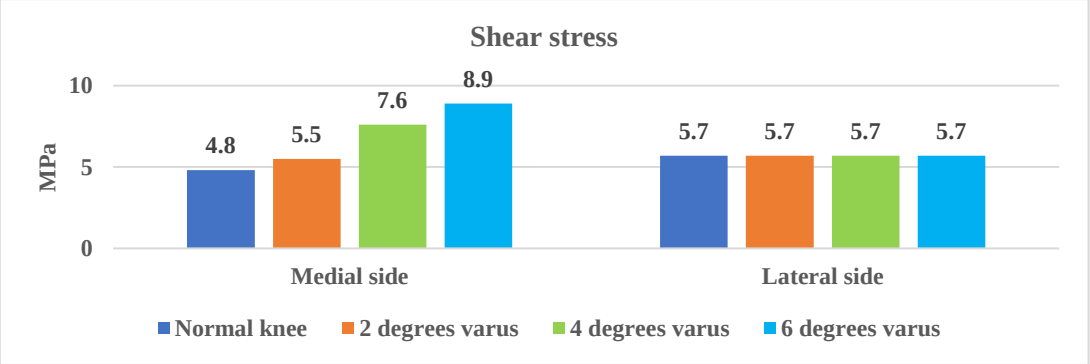

(d)

Fig. 4-12 Tibia cartilage indexes comparison between normal and varus knee (a): Von Mises stress (b): contact pressure (c): compressive stress (d): shear stress

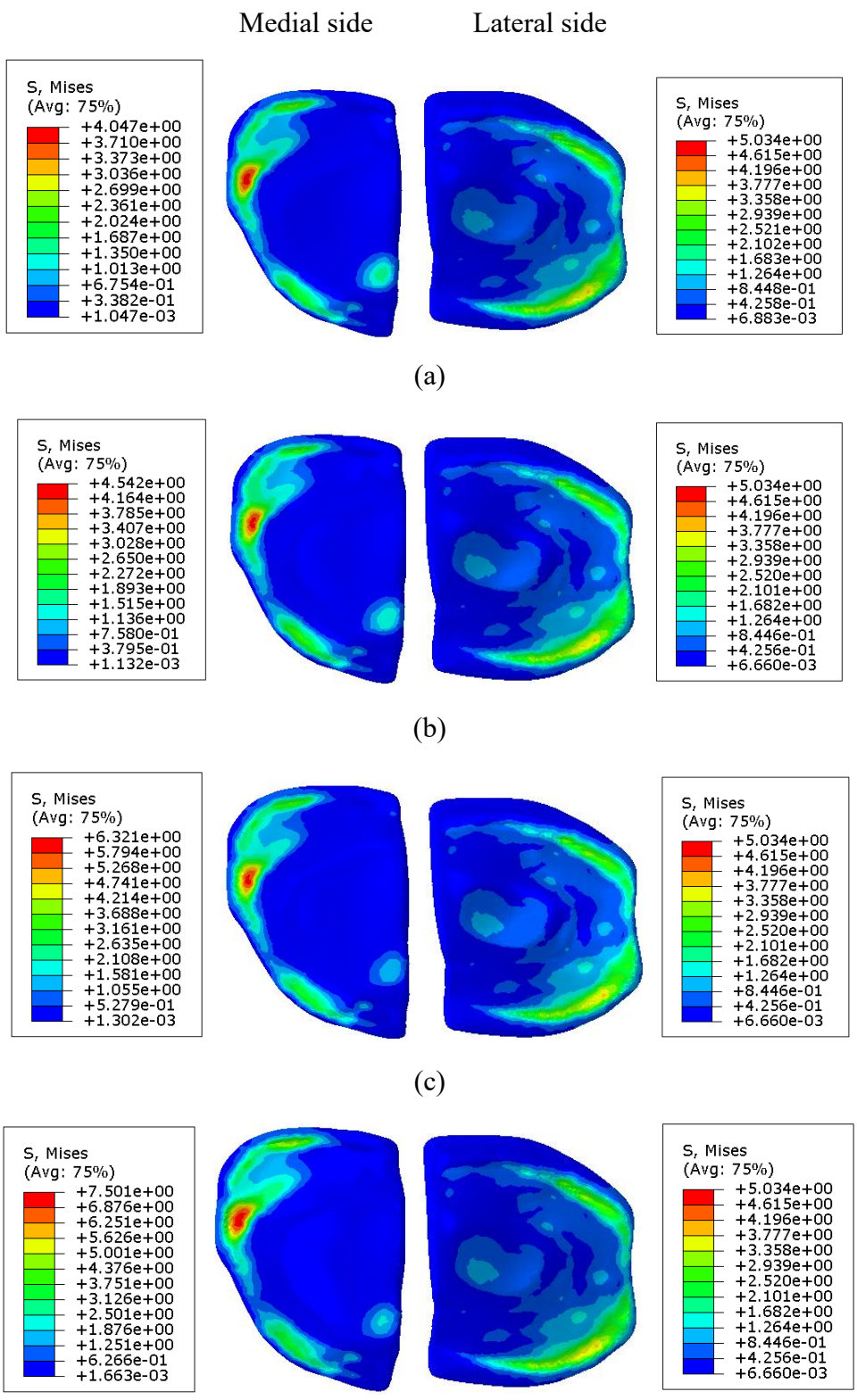

Fig. 4-13 Von Mises stress distribution on tibia cartilage (a): normal knee (b): 2 degrees varus knee (c): 4 degrees varus knee (d): 6 degrees

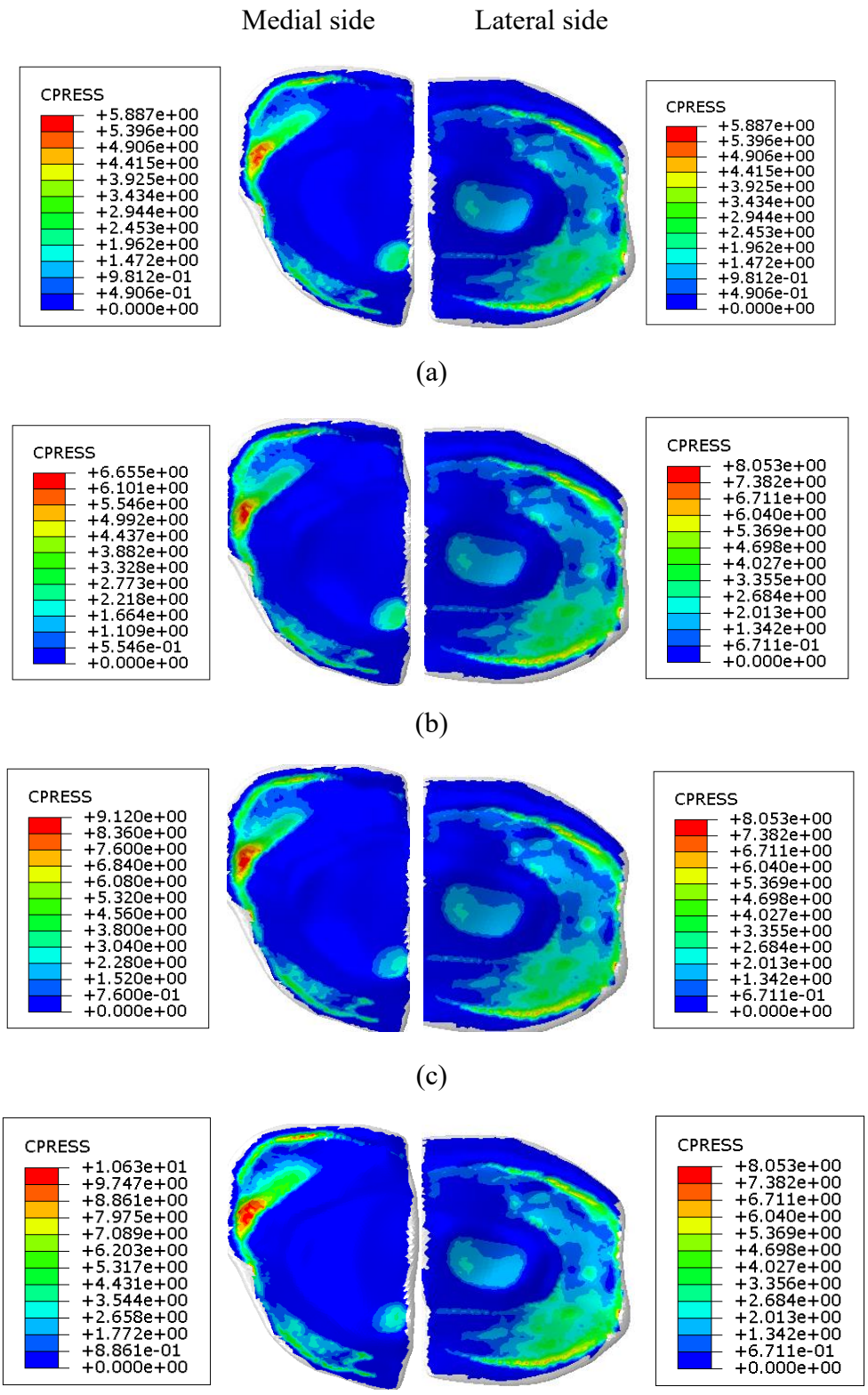

Fig. 4-14 Contact pressure distribution on tibia cartilage (a): normal knee (b): 2 degrees varus knee (c): 4 degrees varus knee (d): 6 degrees

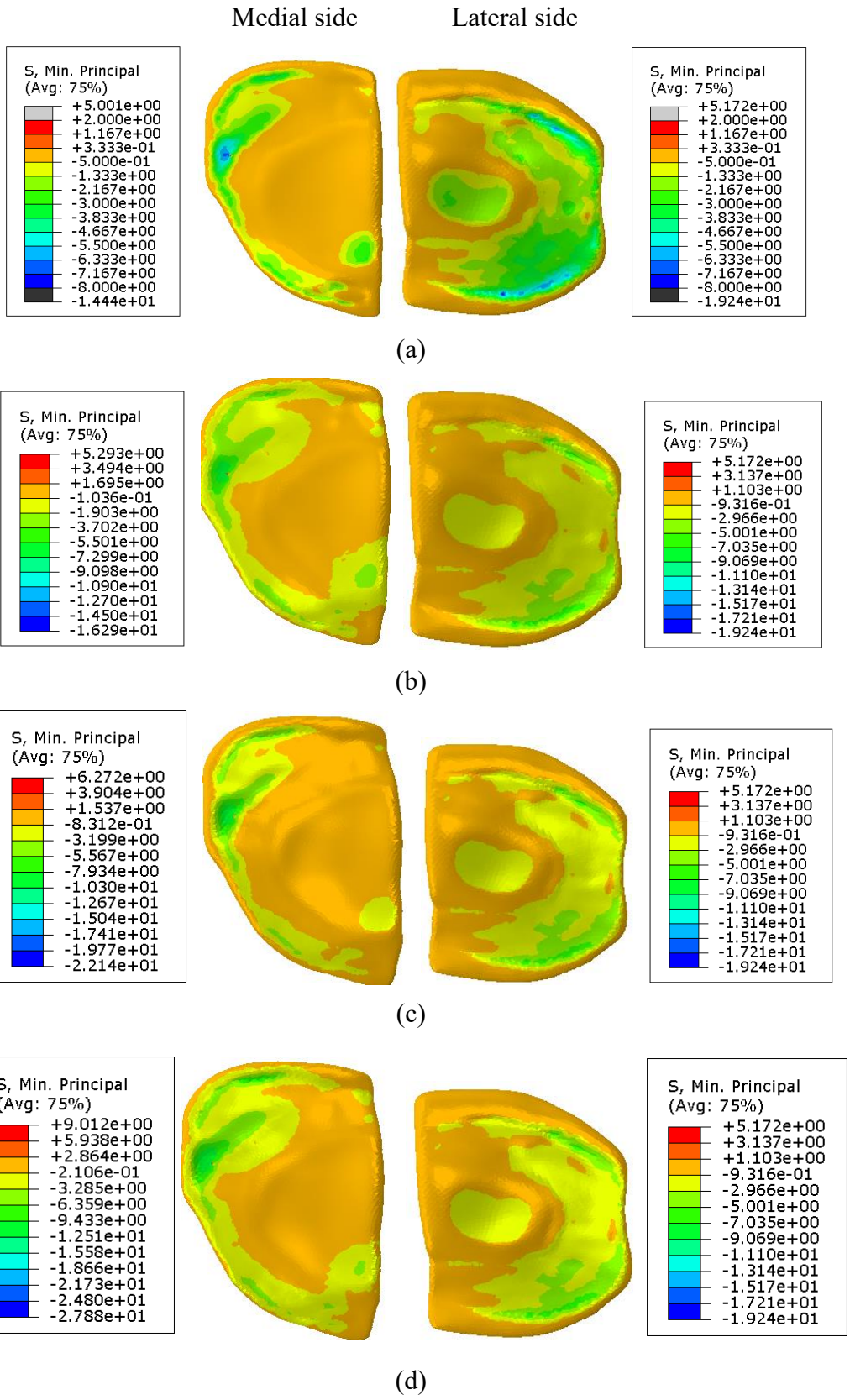

Fig. 4-15 Compressive stress distribution on tibia cartilage (a): normal knee (b): 2 degrees varus knee (c): 4 degrees varus knee (d): 6 degrees

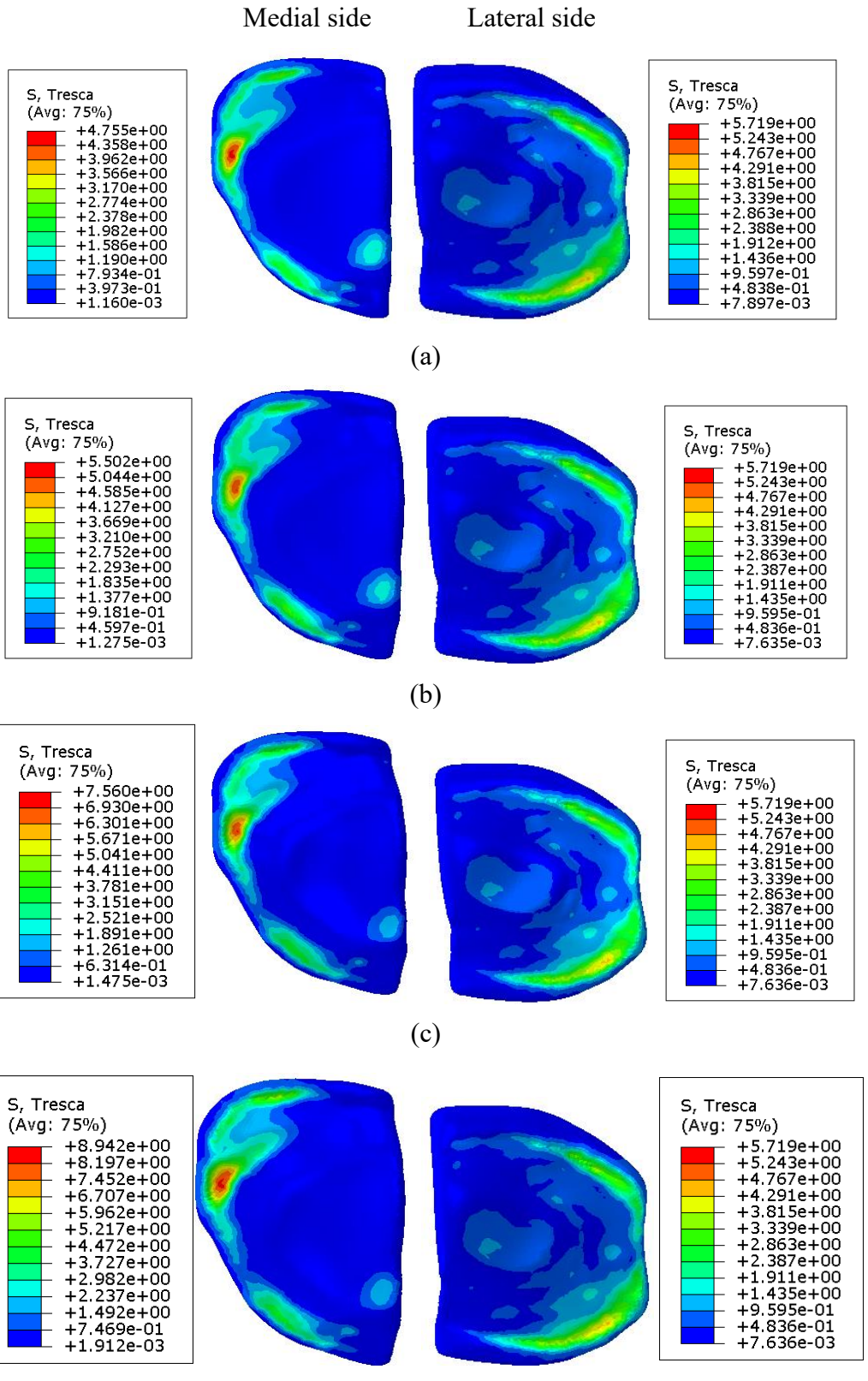

Fig. 4-16 Shear stress distribution on tibia cartilage (a): normal knee (b): 2 degrees varus knee (c): 4 degrees varus knee (d): 6 degrees

4.2.2 Topic II

The interfragmentary movement of the present FE model was consistent with that of previous studies in which the deviation was <0.02. This finding may have been caused by model geometrical differences, individual differences or different correction angles. However, overall, the consistency between the validation result and those of previous studies confirms the ability of the present model to produce convincing results.

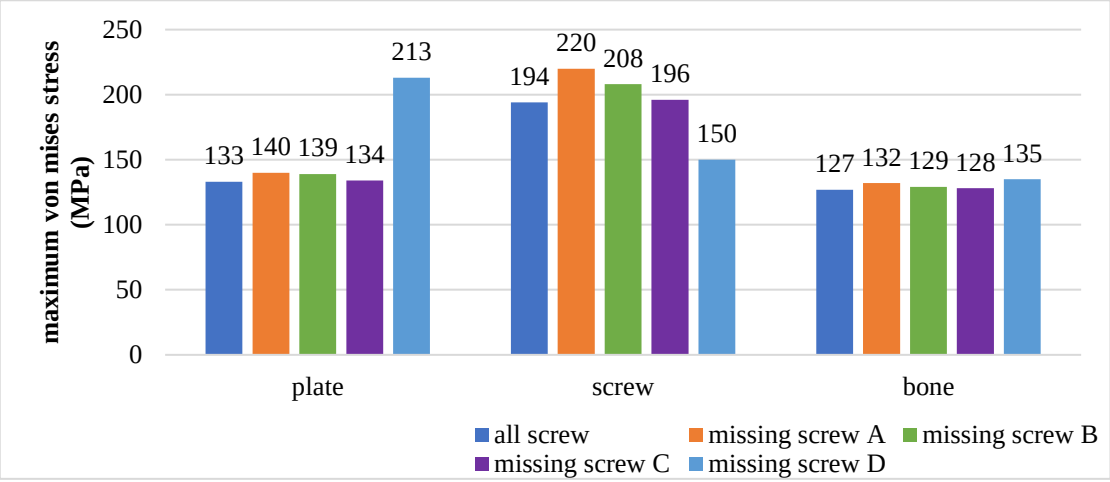

Fig.4-17 Maximum von Mises stress on plate, screw, and bone under different fixation conditions

The maximum stress on the plate was slightly changed when screws A, B, and C were missing (Fig. 4-14). The stress was higher when anyone screw was missing than it was when all screws were present. The stress is highest when screw D was missing, followed by missing screw A, B, and C. The stress was 60% higher when screw D was missing than it was when all screws were present. However, the stress that occurred when a screw was missing was still lower than the yield stress.

The highest stress on the screws occurred when screw A was missing, followed by missing screw B, missing screw C, applying all of the screws, and missing screw D. The stress when missing screw A is 13.4% higher than that when all screws are applied. However, an interesting finding is that the stress on the screws is 22.6% lower when missing screw D than it is when all screws are applied. The stress on the bone

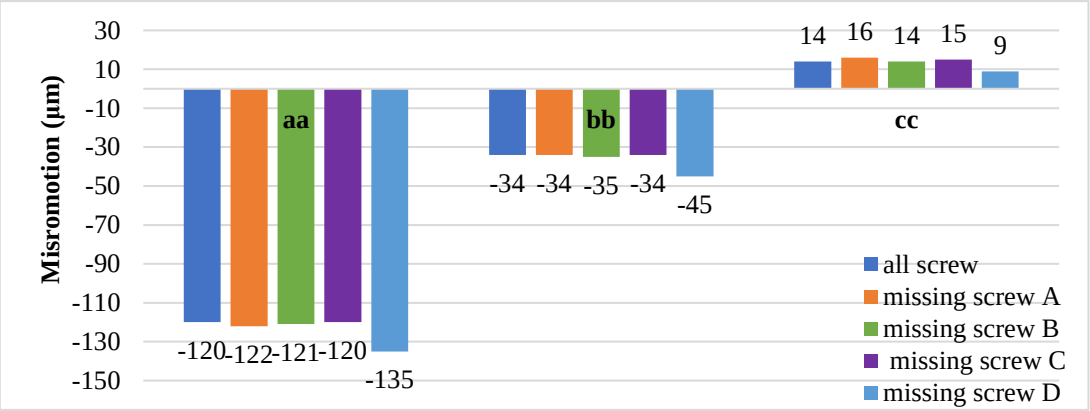

Fig. 4-18 Micromotion of the opening wedge along edges under different fixation conditions.

in missing screw conditions are slightly higher than applying all screws while stress value difference is less than 6%. The maximum stress occurred in the opening wedge hinge point when missing screw D, and the order of maximum stress is missing C, missing B, and missing A, but still lower than the bone (cortical, cancellous) yield stress.

The greatest micromotion was found at edge cc under all fixation conditions. The micromotion change is <2 μm in all fixation scenarios, except when screw D is missing (Fig. 4-16). When missing screw D, the micromotion increased by 12.5% and 32% at edge aa and bb, respectively. Although it decreased 5 μm along edge cc, based on the overall results, the micromotion increased substantially when screw D was missing. Besides, the tension deformation occurred at edge cc, while the compression was exerted at edges aa and bb.

This topic investigated the implant (screw, plate) fixation stability and biomechanical environment change in certain cases. The most important finding of this study was that the stresses on the plate and screw were significantly increased when locking screw D was missing. This increased stress can increase the risk of plate and screw failure. Besides, when the interfragmentary movement was increased, it provides a better bone union environment and decreases the stress shielding effect, however, the plate became relatively unstable when missing one screw. This finding

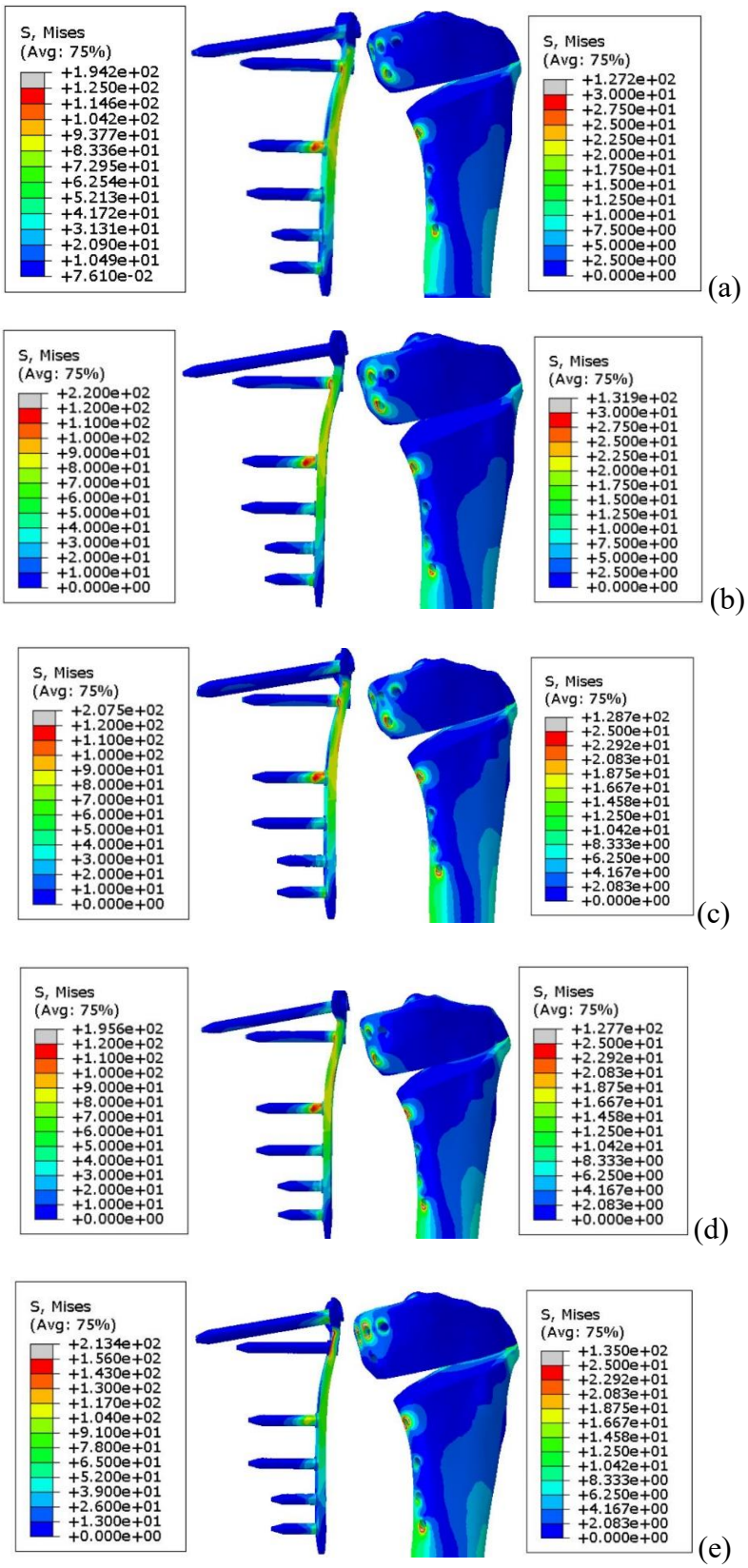

Fig. 4-19 Von Mises stress distribution on TomoFix plate and bone (a): apply all screws (b): missing screw A (c): missing screw B (d): missing screw C (e): missing screw D

can serve as a reference for surgeons performing HTO for patients with special conditions. There must be an essential balance between stability and flexible fixation.

To maintain the correction angle after HTO, it is important to optimize the fixation stability provided by the TomoFix system. If the plate bearing the bulk stress and opening wedge cannot get enough stimulation from the force, delayed bone union or disunion can occur. Pilliar et al.'s study recommended a maximum interfragmentary movement >100 μm for the bone [77]. Several prior studies have shown that high rigid fixation can lead to osteoporosis due to a stress shielding effect [78, 79]. Cales et al. described that the micromotion should be <200 μm between segments in a bony structure stimulated callus formation in early bone union stages [80]. In this study, all of the micromotions were >100 μm and <200 μm. With regard to previous studies, the stress shielding effect will not happen with the TomoFix system when applying all of the locking screws or missing one of the screws (including A, B, C, or D). On the other side, it is beneficial to the bone union to increase the micromotion by 15 μm (from 120 μm to 135 μm). The greatest stress on the bone occurs at the wedge hinge portion, where the stress increased by 6% when screw D was missing. In clinical practice, the potential breakage of the opening hinge is a matter of concern, which may be multifactorial [81, 82]. In this study, the maximum stress at the hinge was increased when screw D was missing. Furthermore, based on the increased stress at the hinge, the authors believe that missing screw D could be a risk factor of the opening wedge hinge breakage.

We also found that the stress on the plate increased by 60% (from 133 MPa to 213 MPa) when screw D was missing. Although this increase does not reach the yield stress of titanium alloy, it could increase the risk of plate breakage during the long period of bone union. One interesting finding is that the greatest stress occurred on screw D in all of screw fixation scenarios. Therefore, screw D failure may be a considerable issue when performing HTO in a patient in whom one locking screw (screw A, B, C, D) must be omitted.

We acknowledge several limitations in this topic. First, the initial compressive stress of the TomoFix plate was not considered. This omission made it extremely

complicated to simulate the HTO procedure using a numerical analysis method. Second, the thread of the screw was neglected because the bonding contact can effectively simulate the screw-bone interaction. Third, this study focused only on the tibia. Therefore, our findings may not be generalizable to other bones, cartilage, or ligaments.

This topic investigated the fixation stability and stress on the TomoFix system and bone in different fix conditions. The results suggest that the fixation stability and biomechanical environment are all slightly influenced by the absence of screw A, B, or C, However, missing locking screw D will be the risk of hinge breakage. We suggest that increasing the protection time (partial weight duration) when missing one locking screw to decrease the risk of screw breakage and hinge breakage.

Chapter 5 Conclusions and future work

5.1 Conclusion

In this study, one intact normal knee FE model and one after-HTO tibia FE model that fixed with TomoFix were developed. The normal knee biomechanical environment change and the plate fixed stability were investigated.

The varus deformity strongly influences the stress and contact pressure distribution on knee medial and lateral compartment, it could be the risk factor of OA. By comparing the indexes between the varus knee and normal, based on the results, we believe that HTO can balance the biomechanical environment effectively.

TomoFix plate fixation stability and biomechanical environment are all slightly influenced by the absence of screw A, B, or C, However, missing locking screw D will be the risk of hinge breakage. We suggest that increasing the protection time (partial weight duration) when missing one locking screw to decrease the risk of screw breakage and hinge breakage.

Another achievement of this study is that a validated intact knee model was developed. This model not only can be used to qualify the stress and contact pressure of varus deformity but also can be used to research other topics about the knee joint. We also created a new method to get a certain varus or valgus angle with the normal knee model. Compare to build different models with the image data of patients, our method is more convenient and efficient.

5.2 Future work

In this study, we acknowledge several limitations. First, all the soft tissues and bone material properties were assumed to be isotropic and linear elastic. Second, for the after-HTO model, the open-wedge was not created. Third, in topic II, all the soft tissues were not included. Forth, the screw thread was neglected.

In the future, we will overcome all the limitations to achieve better results.

Reference

[1] March L, Smith EU, Hoy DG, Cross MJ, Sanchez-Riera L, Blyth F, Buchbinder R, Vos T, Woolf AD (June 2014). "Burden of disability due to musculoskeletal (MSK) disorders". Best Practice & Research. Clinical Rheumatology. 28 (3): 353–66.

[2] National Institute of Arthritis and Musculoskeletal and Skin Diseases. April 2015. Archived from the original on 18 May 2015. Retrieved 13 May 2015.

[3] Brandt KD, Dieppe P, Radin E (January 2009). "Etiopathogenesis of osteoarthritis". The Medical Clinics of North America. 93 (1): 1–24, xv.

[4] Felson, D. T. (2000). Osteoarthritis: New Insights. Part 1: The Disease and Its Risk Factors. Annals of Internal Medicine,2000, 133(8):635-646

[5] Dunlop D D, Manheim L M, Song J, et al. Arthritis prevalenc and activity limitations in older adults[J]. Aithritis&Rheumatism, 2001, 44(1):212-221.

[6] Lawrence J S. Rheumatismin population[M]. London: William Heinemann Medical books, 1977

[7] Riegger-Krugh, C., et al., Tibiofemoral contact pressures in degenerative joint disease. Clinical Orthopaedics and Related Research, 1998(348): p. 233-245.

[8] Turner M J, Clough R W, Martin H C, et al. Stiffness and deflection analysis of complex structures[J]. Journal of the Aeronautical Sciences.1956, 23(9): 805-823.

[9] Brekelmans W A M, Poort H W, Slooff T J J H. A new method to analyze the mechanical behaviour of skeletal parts[J]. Acta Orthopaedica Scandinav, 1972,43(5): 301-317.

[10] Belytschko T, Kulak R F, Schultz A B. Finite element stress analysis of an intervertebral disc[J]. Journal of Biomechanics, 1974, 7(3): 277-285.

[11] Rybicki E F, Simonen F A, Weis E B. On the mathematical analysis of stress in the human femur[J]. Journal of Biomechanics, 1972, 5(2): 203-215.

[12] Bendjaballah M Z, Shirazi-Adl A, Zukor D J. Biomechanical response of the passive human knee joint under anterior-posterior forces[J]. Clinical Biomechanics,1998, 13(8): 625-633.

[13] Donahue H L, Hull M L, Rashid M M, et al. A finite element model of the human knee joint for the study of tibio-femoral contact. Journal of Biomechanical Engineering, 2002, 124(3): 273-280.

[14] Dong Y F, Hu G H, Zhang L L, et al. Accurate 3D reconstruction of subject-specific knee finite element model to simulate the articular cartilage defects[J]. Journal of Shanghai Jiaotong University (Science), 2011, 16(5):620-627.

[15] Nattapon C, Pruettha N, Bancha C, et al. A finite element study of stress distributions in normal and osteoarthritic knee joints[J]. Journal of the Medical Association of Thailand, 2009, 92(6): 97-103.

[16] Ji Y B, Kyung S P, Jong K S, et al. Biomechanical analysis of the effects of medial meniscectomyon degenerative osteoarthritis[J]. Medical & Biological Engineering& Computing, 2012, 50(1): 53-60.

[17] Homyk A, Orsi A, Wibby S, et al. Failure locus of the anterior cruciate ligament: 3D finite element analysis[J]. Computer Methods in Biomechanics and Biomedical Engineering, 2012, 15(8): 865-874.

[18] E. pena, B. Calvo, et al. A three-demensional finite element analysis of combined behavior of ligaments and menisci in the healthy human knee joint[J] journal of biomechanics 39 (2006) 1686-1701

[19] Yong-Gon Koh, Juyun son, et al. Biomechanical evaluation od opening-wedge high tibial osteotomy with composite materials using finite-element analysis[J]. The knee 25(2018) 977-987

[20] Yen-Nien Chen et al. biomechanical investigation of the type and configuration of screws used in high tibial osteotomy with titanium locking plate and screw fixation[J]. Journal of orthopaedic surgery and research(2019)

[21] Yang R S, Lin H J. Contact stress on polyethylene components of a new rotating hinge with a spherical contact surface[J]. Clinical Biomechanics, 2001, 16(6):540-546.

[22] Tomaso V, Francesco M, Dario G, et a1. Contact stresses and fatigue life in a knee prosthesis: comparison between in vitro measurements and computational simulations[J]. Journal of Biomechanics, 2004, 37(1): 45-53.

[23] Bischoff J E, Hertzler J S, Mason J J. Patellofemoral interactions in walking, stair ascent, and stair descent using a virtual patella model[J]. Journal of Biomechanics. 2009, 42(11): 1678-1684.

[24] Marjian B, Sdahari B B, Mohd R H, et al. Finite element analysis of the effect of shape memory alloy on the stress distribution and contact pressure in total knee replacement [J]. Trends in Biomaterials and Artificial Organs, 2011, 25(3): 95-100.

[25] Jessica M. Hooper. Peter Walker, et al. Biomechanical Implications of an Oblique Knee Joint Line. The Journal of Knee Surgery, 2017, 31(08), 761–766.

[26] Kwang-Jun, Young Bong Ko, et al. Analysis of Knee Joint Line Obliquity after High Tibial Osteotomy. The Journal of Knee Surgery, 2016, 29(08), 649–657.

[27] Jonathan Hutt, Vincent Masse, et al. Functional joint line obliquity after kinematic total knee arthroplasty. International Orthopaedics, 2015, 40(1), 29–34.

[28] Mitsuaki Kubota, Youngji Kim, et al. The actual knee function was not influenced by joint line obliquity after open-wedge high tibial osteotomy. SICOT-J 2020, 6, 4

[29] Yong-Gon Koh, Jin-Ah Lee, et al. Design optimization of high tibial osteotomy plates using finite element analysis for improved biomechanical effect. Journal of Orthopaedic Surgery and Research. 2019, 14:219

[30] Schallberger, A., et al., High tibial valgus osteotomy in unicompartmental medial osteoarthritis of the knee: a retrospective follow-up study over 13-21 years. Knee Surgery Sports Traumatology Arthroscopy, 2011. 19(1): p. 122-127.

[31] Jackson JP, Waugh W. Tibial osteotomy for osteoarthritis of the knee. J Bone Joint Surg Br. 1961;43:746-751

[32] Coventry MB. Osteotomy about the knee for degenerative and rheumatoid arthritis. J Bone Joint Surg Am.1973;55:23-48.

[33] Blecha LD, Zambelli PY, Ramaniraka NA, Bourban PE, Manson JA, Pioletti DP. How plate positioning impacts the biomechanics of the open wedge tibial osteotomy; a finite element analysis. Comput Methods Biomech Biomed Engin. 2005;8(5):307–13.

[34] Coventry MB. Osteotomy of the upper portion of the tibia for degenerative Arthritis of the knee: A preliminary report. The journal of Bone&Joint Surgery. 47(5):984-990, July 1965

[35] Benzakour, T., et al., High tibial osteotomy for medial osteoarthritis of the knee: 15 years follow-up. International Orthopaedics, 2010. 34(2): p. 209-215.

[36] Amendola, A. and D.E. Bonasia, Results of high tibial osteotomy: review of the literature. International Orthopaedics, 2010. 34(2): p. 155-160.

[37] Smith, T.O., et al., Opening- or closing-wedged high tibial osteotomy: A meta-analysis of clinical and radiological outcomes. Knee, 2011. 18(6): p.361-368.

[38] Coventry, M.B., UPPER TIBIAL OSTEOTOMY. Clinical Orthopaedics and Related Research, 1984(182): p. 46-52.

[39] Miniaci A, FT Ballmer, PM Ballmer, RP Jakob. “Proximal tibial osteotomy: a new fixation device.” Clin Orthop Relat Res (246) (1989): 250–9.

[40] TomoFix Medial High Tibial Plate (MHT) Surgical Technique DePuy Synthes

[41] Han SB, Lee DH, Shetty GM, Chae DJ, Song JG, Nha KW. A “safe zone” in medial open-wedge high tibia osteotomy to prevent lateral cortex fracture. Knee Surg Sports Traumatol Arthrosc. 2013; 21:90–5

[42] Han SB, Bae JH, Lee SJ, Jung TG, Kim KH, Kwon JH, et al. Biomechanical properties of a new anatomical locking metal block plate for opening wedge high tibial osteotomy: uniplane osteotomy. Knee Surg Relat Res. 2014;26(3):155–61.

[43] Stoffel K, Stachowiak G, Kuster M. Open wedge high tibial osteotomy: biomechanical investigation of the modified Arthrex Osteotomy Plate (Puddu Plate) and the TomoFix Plate. Clin Biomech (Bristol, Avon) 2004;19:944–50

[44] Diffo Kaze A, Maas S, Waldmann D, Zilian A, Dueck K, Pape D. Biomechanical properties of five different currently used implants for open-wedge high tibial osteotomy. J Exp Orthop. 2015;2(1):14.

[45] Roderer G, Gebhard F, Duerselen L, Ignatius A, Claes L. Delayed bone healing following high tibial osteotomy related to increased implant stiffness in locked plating. Injury. 2014;45(10):1648–52.

[46] Luo CA, Hua SY, Lin SC, Chen CM, Tseng CS. Stress and stability comparison between different systems for high tibial osteotomies. BMC Musculoskelet Disord 2013;14:110

[47] Cotz Roderer, Florian Gebhard. Delayed bone healing following high tibial osteotomy related to increased implant stiffness in locked plating. Injury. Int. J. Care Injured 45 (2014) 1648- 1652

[48] The effects of tibia profile, distraction angle, and kne load on wedge instability and hinge fracture: A finite element study. Medical engineering and physics 42 (2017) 48-54

[49] Chen YN, Chang CW, Lin CW, Wang CW, Peng YT, Chang CH, Li CT. Numerical investigation of fracture impaction in proximal humeral fracture fixation with locking plate and intramedullary nail. Int Orthop. 2017;41: 1471–80.

[50] Chen YN, Lee PY, Chang CH, Chang CW, Ho YH, Li CT, Peng YT. Computational comparison of tibial diaphyseal fractures fixed with various degrees of prebending of titanium elastic nails and with and without end caps. Injury. 2016;47:2339–46.

[51] Chen YN, Lee PY, Chang CW, Ho YH, Peng YT, Chang CH, Li CT. Biomechanical investigation of titanium elastic nail prebending for treating diaphyseal long bone fractures. Australas Phys Eng Sci Med. 2017;40:115–26.

[52] Chang CW, Chen YN, Li CT, Chung YH, Chang CH, Peng YT. Role of screw proximity in the fixation of transverse patellar fractures with screws and a wire. J Orthop Surg (Hong Kong). 2018

[53] Raja Izaham RM, Abdul Kadir MR, Abdul Rashid AH, Hossain MG, Kamarul T. Finite element analysis of Puddu and Tomofix plate fixation for open wedge high tibial osteotomy. Injury. 2012;43(6):898–902.

[54] Luo CA, Hua SY, Lin SC, Chen CM, Tseng CS. Stress and stability comparison between different systems for high tibial osteotomies. BMC Musculoskelet Disord. 2013;14:110.

[55] Luo CA, Lin SC, Hwa SY, Chen CM, Tseng CS. Biomechanical effects of plate area and locking screw on medial open tibial osteotomy. Comput Methods Biomech Biomed Engin. 2015;18(12):1263–71.

[56] Noyes FR, Barber-Westin SD, Hewett TE. High tibial osteotomy and ligament reconstruction for varus angulated anterior cruciate ligament-deficient knees. Am J Sports Med. 2000;28(3):282–96.

[57] Hankemeier S, Hufner T, Wang G, Kendoff D, Zeichen J, Zheng G, et al. Navigated open-wedge high tibial osteotomy: advantages and disadvantages compared to the conventional technique in a cadaver study. Knee Surg Sports Traumatol Arthrosc. 2006;14(10):917–21.

[58] Donahue, T.L.H., et al., A finite element model of the human knee joint for the study of tibio-femoral contact. Journal of Biomechanical Engineering-Transactions of the Asme, 2002. 124(3): p. 273-280.

[59] N. Yang, P. Canavan, H. Nayeb-Hashemi, B. Najafi and A. Vaziri, "Protocal for constructing subject-specific biomechanical models of knee joint," Computer Methods in Biomechanics and Biomedical Engineering, vol. 13, no. 5, pp. 589-603, 2010.

[60] Y. Guo, X. Zhang and W. Chen, "Three-dimensional finite element simulation of total knee joint in gait cycle," Acta Mechanica Solida Sinica, vol. 22, no. 4, pp. 347-351, 2009.

[61] S. Woo, S. Abramowitch, R. Kilger and R. Liang, "Biomechanics of knee ligaments: injury, healing, and repairt," Journal of Biomechanics, vol. 39, pp. 1-20, 2006.

[62] D. Bartel, D. Davy and T. Keaveny, Orthopaedic Biomechanics: Mechanics and Design in Musculoskeletal Systems, Upper Saddle River, NJ: Pearson Education, Inc., 2006.

[63] Hoffler CE, Moore KE, Kozloff K, Zysset PK, Goldstein SA. Age, gender, and bone lamellae elastic moduli. J Orthop Res. 2000;18(3):432–7.

[64] Kazimoglu C, Akdogan Y, Sener M, Kurtulmus A, Karapinar H, Uzun B.Which is the best fixation method for lateral cortex disruption in the medial open wedgehigh tibial osteotomy? A biomechanical study. Knee 2008;15:305–8.

[65]Li, G., et al., A validated three-dimensional computational model of a human knee joint. Journal of Biomechanical Engineering-Transactions of the Asme, 1999. 121(6): p. 657-662.

[66] Kang KT, Kim SH, Son J, Lee YH, Chun HJ. Computational model-based probabilistic analysis of in vivo material properties for ligament stiffness using the laxity test and computed tomography. J Mater Sci Mater Med. 2016;27(12):183.

[67] Golovakha ML, Orljanski W, Benedetto KP, Panchenko S, Buchler P, Henle P, et al. Comparison of theoretical fixation stability of three devices employed in medial opening wedge high tibial osteotomy: a finite element analysis. BMC Musculoskelet Disord. 2014;15:230.

[68] Walker, P.S., Erkman, M.J., 1975. The role of the menisci in force transmission across the knee. Clinical Orthopaedics and Related Research 109, 184–192.

[69] Dong, Y., Hu, G., Dong, Y., Hu, Y., & Xu, Q. (2013). The effect of meniscal tears and resultant partial meniscectomies on the knee contact stresses: a finite element analysis. Computer Methods in Biomechanics and Biomedical Engineering, 17(13), 1452–1463.

[70] Bendjaballah, M.Z., Shirazi-adl, A., Zukor, D.J., 1995. Biomechanics of the human knee joint in compression: reconstruction, mesh generation and finite element analysis. Knee 2, 69–79.

[71] Fukubayashi, T., Kurosawa, H., 1980. The contact area and pressure distribution pattern of the knee. Acta Orthopaedics Scandinavian 51, 871–879.

[72] Cotz Roderer, Florian Gebhard. Delayed bone healing following high tibial osteotomy related to increased implant stiffness in locked plating. Injury. Int. J. Care Injured 45 (2014) 1648- 1652

[73] Hunter DJ, Zhang YQ, Niu JB, Tu X, Amin S, Clancy M, Guermazi A, Grigorian M, Gale D, Felson DT. 2006. The association of meniscal pathologic changes with cartilage loss in symptomatic knee osteoarthritis. Arthritis Rheum. 54(3):795–801.

[74] Sharma L, Eckstein F, Song J, Guermazi A, Prasad P, Kapoor D, Cahue S, Marshall M, Hudelmaier M, Dunlop D. 2008. Relationship of meniscal damage, meniscal extrusion, malalignment, and joint laxity to subsequent cartilage loss in osteoarthritic knees. Arthritis Rheum. 58(6):1716–1726.

[75] Englund M, Guermazi A, Roemer FW, Aliabadi P, Yang M, Lewis CE, Torner J, Nevitt MC, Sack B, Felson DT. 2009. Meniscal tear in knees without surgery and the development of radiographic osteoarthritis among middle-aged and elderly persons: the multicenter osteoarthritis study. Arthritis Rheum. 60(3):831–839.

[76] Lee SJ, Aadalen KJ, Malaviya P, Lorenz EP, Hayden JK, Farr J, Kang RW, Cole BJ. 2006. Tibiofemoral contact mechanics after serial medial meniscectomies in the human cadaveric knee. Am J Sports Med. 34(8):1334–1344.

[77] Pilliar RM, Lee JM, Maniatopoulos C. Observations on the effect of movement on bone ingrowth into porous-surfaced implants. Clin Orthop Relat Res. 1986;208:108-13.

[78] Benli S, Aksoy S, Havitcioglu H, Kucuk M. Evaluation of bone plate with low-stiffness material in terms of stress distribution. J Biomech. 2008;41(15):3229–35.

[79] Fan Y, Xiu K, Duan H, Zhang M. Biomechanical and histological evaluation of the application of biodegradable poly-L-lactic cushion to the plate internal fixation for bone fracture healing. Clin Biomech (Bristol, Avon). 2008;23(Suppl 1):S7–s16.

[80] Claes LE, Heigele CA, Neidlinger-Wilke C, Kaspar D, Seidl W, Margevicius KJ,et al. Effects of mechanical factors on the fracture healing process. Clin Orthop Relat Res. 1998;355(Suppl):S132-47.

[81] Nakamura R, Komatsu N, Fujita K, Kuroda K, Takahashi M, Omi R, Katsuki Y, Tsuchiya H. Appropriate hinge position for prevention of unstable lateral hinge fracture in open wedge high tibial osteotomy. Bone Joint J. 2017;99-B:1313–8.

[82] Lee OS, Lee YS. Diagnostic value of computed tomography and risk factors for lateral hinge fracture in the open wedge high tibial osteotomy. Arthroscopy. 2018;34:1032–43.